Journal of Petroleum and Gas Engineering

Volume 5 Number 5 November, 2014

ISSN-2141-2677

Academic Journals

www.academicjournals.org/jpge

ABOUT JPGE

Journal of Petroleum and Gas Engineering (JPGE) is an open access journal that provides rapid publication (monthly) of articles in all areas of the subject such as Petroleum geology, reservoir simulation, enhanced oil recovery, Subsurface analysis, Drilling Technology etc.

The Journal welcomes the submission of manuscripts that meet the general criteria of significance and scientific excellence. Papers will be published shortly after acceptance. All articles published in JPGE are peer-reviewed.

Journal of Petroleum and Gas Engineering is published monthly (one volume per year) by Academic Journals.

Contact Us

Editorial Office: jpge@academicjournals.org

Help Desk: helpdesk@academicjournals.org

Website: http://www.academicjournals.org/journal/JPGE

Submit manuscript online http://ms.academicjournals.me/

Journal of Petroleum and Gas

Table of Contents: Volume 5 Number 5 November 2014

ARTICLES

Research Articles

academicJournals

Vol. 5(5), pp. 49-56, November, 2014
DOI: 10.5897/JPGE2014.0200
Article Number: 937A25F48317
ISSN 2141-2677

http://www.academicjournals.org/JPGE

Journal of Petroleum and Gas Engineering

Full Length Research Paper

Investigation of hydraulic fracture optimization in on Infill well in low permeability reservoirs

Wang Wendong, Su Yuliang*, Zhou Shiyu, Yuan Bin and Shang Yangyang

School of Petroleum Engineering, China University of Petroleum (East China), Qingdao, Shandong 266580, China.

Received 8 July, 2014; Accepted 10 October, 2014

Well infilling has become an effective approach to enhance oil recovery (EOR) for many years. Closely spaced wells and water injections can help maintain reservoir pressure and enlarge producing pressure drop, which are beneficial to the low permeability reservoir development. After more than 20 years of water injection in the Ansai low permeability oil reservoir (Changqing Oil Field, China), water cut of wells now increases rapidly and the production rate decreases greatly. The primary recovery scheme and well spacing are no longer efficient. Pilot well pattern adjustments including converting, infilling and hydraulic fracturing have been adopted. Some wells achieved good results; however, due to the imperfect fracturing design, most fractured wells water broke through along fractures and led to water channeling. Meanwhile, fracture reorientation has been monitored, indicating that an integral readjustment is necessary, and in case of the probability of fracture reorientation, the process of redesigning infill well pattern and fracturing optimization should be carefully discussed before hydraulic fracture stimulation. In this paper, reservoir simulation models have been conducted, using near wellbore modeling (NWM) technology. New fractures with different orientations are incorporated in the reservoir models to better understand the involving infill wells' performance. Numerical simulations indicate that infill wells inside inverted nine-spot pattern can be divided into several types and that each type has different production characteristics as well as optimal fracture length scope. Furthermore, the new fracture orientation and length can change the direction of mainstream line. We also give the theoretical production type curves where all kinds of fracture orientation have been considered. According to the simulation results, concept of minimum-risk optimization (MRO) and fracturing safe interval (FSI) have been put forward to estimate the optimal fracturing design for infill wells when fracture reorientation cannot be precisely detected. This design cannot only guarantee good well pattern performance, but also minimize the risks associated with difficulty in pre-determining infill fracture reorientation.

Key words: Low permeability reservoir, infill well, fracture reorientation, fracture length, minimum-risk optimization (MRO), fracturing safe interval (FSI).

INTRODUCTION

Infill drilling and fracturing technology is considered to be an effective method to enhance low permeability oil field. Before 1960, ultimate recovery was supposed to be unrelated to well spacing (Ching et at., 1989). In 1980,

*Corresponding author. E-mail: suyuliang@upc.edu.cn.

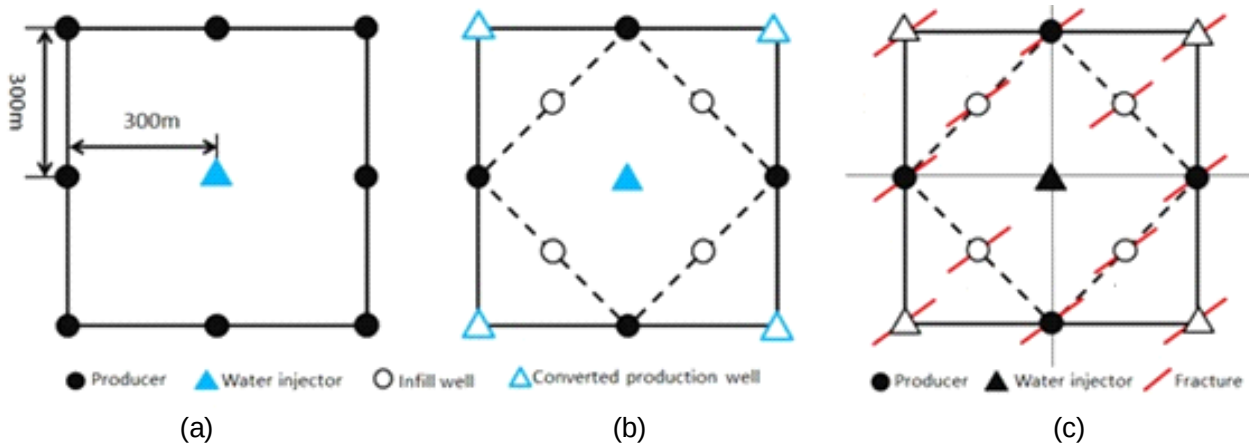

Figure 1. Schematic diagrams of well pattern adjustment: (a) Original invert nine point well pattern; (b) infilling well of invert nine point well patterns; (c) infilling well design fracture orientation. Diagonal well pattern adjustment has been designed to control the water channeling and to promote production, in which well spacing reduces to 240 to 260 m with row spacing 160 to 190 m. All the infill wells have been hydraulically fractured, which fracture orientation N67°E, fractures length 240 m, fracture conductivity 200 × 10^{-3} μm^2·m.

Van Everdingen and Kriss (1980) stated that infill drilling could be adopted in enhanced oil recovery (EOR), however their study was not convincing enough due to inadequate data. Barber and George (1983) published case studies from Texas, Oklahoma and Illinois, proving that infill drilling could increase oil production in combination with well pattern adjustments. In one example presented by these authors, wells' pattern has changed from a peripheral pattern to an inverted nine-spot with infill wells accounting for 68% of the overall daily production. In 1989, Ching et al. (1989) made the general statement that infill drilling in carbonate reservoirs can noticeably increase production during water flooding. Hydraulic fractures are usually assumed to propagate along the maximum stress direction with consequent impact on well pattern design. Hidayati et al. (2001) and Schutjens and Kuvshinov (2010) thought that the injection or production of large volumes of fluid into or from a reservoir can significantly change the effective *in situ* stress distribution, which could deviate hydraulic fractures from its forecasted path. The magnitude of reorientation depends on pressure gradients and thus, it is controlled by injection/production rates and pore pressure variations in the reservoir (Zhai and Sharma, 2007). The radius of fracture reorientation has been investigated by analytical and experimental methods (Deimbacher et al., 1993; Rod 2005). Besides vertical drilling, studies about stress reorientation around horizontal wellbores were also conducted (Hidayati et al., 2001; Singh et al., 2008; Sharma et al., 2008).

As for the probability of fracture reorientation, Wright (1995) found that water flood related to secondary recovery in Diatomite reservoirs have caused directions of infill hydraulic fractures to rotate with more than 60° away from the original direction. Weijers (1999) studied the fracture reorientation in steam injection wells and proposed that the induced fractures grew predominantly along the direction that was 45° off of the preferred fracture plane in South Belridge, Lost Hills, and Cymric fields. Other studies also showed that the azimuth of reoriented fractures is usually between 0° and 90° (Wright, 1994; Wolhart, 2007).

Roussel et al. (2013) used a numerical model of fracture propagation from an infill horizontal well drilled within stress field affected by prior production from offset wells to simulate the occurrence of stress reversal within the infill region and demonstrated its impact on the direction of fractures propagated from an infill well. A window of opportunity has been proposed to improve the stimulation efficiency by fracturing the infill well around (ideally slightly before) the time when principal horizontal stresses change directions. They also suggested considering the risk of stress reversal before infill operations.

In the Ansai low permeability reservoir, the EOR development hinges on infilling vertical well stimulation.

The primary well pattern in the pilot area was inverted square nine-spot, whose well space is 300 × 300m (Figure 1a). After more than 20 years of water injection, well pattern designed for primary recovery are no longer efficient. Water cut of vertical wells increases rapidly and the production rate decreases accordingly. To enhance efficiency of water flooding, the pilot test well pattern adjustments including converting, infilling and hydraulic fracturing have been adopted (Figure 1b and c).

Even though well infilling and hydraulic fracturing in pilot area significantly increased the well group production, some problems still exist. Twenty-four (24) infill wells were put into production after fracturing in the first stage, and early water breakthrough happened in

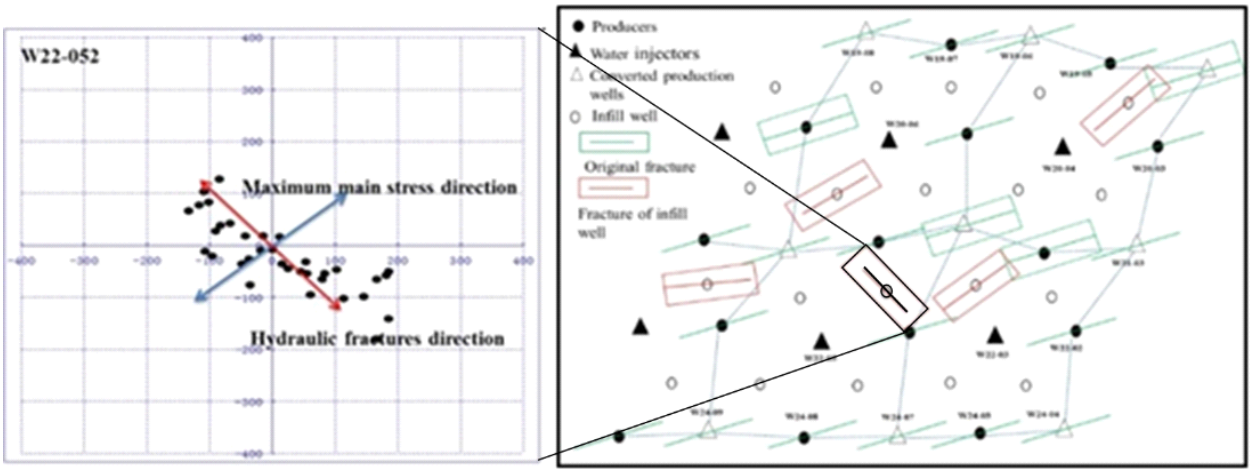

Figure 2. Microseismic monitoring of fracture orientation in Ansai reservoir pilot area: detail of the W22-052 infilling fractured well showing the fracture orientation severely deflected from the original maximum main stress direction (left figure); overall micro-seismic monitoring results of Ansai pilot test area, the red frame represent infill fractured wells. Majority of infill wells fracture deviate from maximum stress direction very small, but still have some infill well deflect 60~90°.

most of new infill wells. About 80% wells seriously flooded after a short time production, reaching 90% water cut at the beginning of development. Since the fracture treatment was not optimized in advance, the fracture parameters for infill wells in the pilot area are proved to be unsuitable. Meanwhile, micro-seismic monitoring indicates that hydraulic fractures of infill wells do not always extend along the maximum stress direction, implying reorientation of the infill wells' fractures (Figure 2). One of the most striking differences between W22-052 and any other infilling wells is fractures' orientation and fractures' length. However, evaluation of the fracture direction was not very insightful due to the diverse stress variations from region to region at each infilling well.

EXPERIMENTAL DESIGN

Infill well drainage patterns

Reservoir simulation model for Ansai oil field was built and calibrated by history matching. To further understand the drainage patterns and flow behaviors of infill well with different fracture orientations in inverted nine-spot well pattern, series of streamline three-dimensional theoretical model were conducted by using local grid refinement method (LGR). Two cases are considered respectively: firstly, no infill well fracture reorientation happens, in other words, all well fractures remained consistent; next is the infill fractures deflection at 90°. Models are calibrated using properties of the Ansai low permeability oil reservoir (Table 1).

As shown in Figure 3, streamline distributions between injection and production wells are not evenly, and infill fracture orientation could significantly affect fluid flow behavior. When the infill fracture orientation is perpendicular to the production-injection connection line, the waterlines distributed uniformly on both sides of infill Well A (Figure 3i). However, due to the fracture deflection, the streamline becomes denser at the tip of the injector well fractures, which could enhance the sweep efficiency around the Well D (Figure 3ii). In these two cases, as long as the infill fracture orientation along with the injection wells or inject waterline, the water-cut of the production well increases significantly. For example, Well B production is more sensitive to the fracture reorientation, which increases the reservoir heterogeneity in small region.

Fracture reorientation is a complex phenomenon during hydraulic fracture stimulation. Principal stress direction may change due to the pore-elastic effects (Hagemann et al., 2012) and water injections (Perapon et al., 2012). In this paper, series reservoir simulation models were conducted to address the Minimum-risk Optimization (MRO) of infill fractures when fractures orientation cannot be pre-determined. With further investigation of drainage patterns between Wells A and B, we find that the relative location relationship between infilling wells and injector wells affects the optimal infill fracture designs. For example, Wells A and B should be treated separately during the hydraulic fractures design, which may have different optimal fracture properties.

RESULTS AND DISCUSSION

Infill well fracture half-length optimization

Cases without fracture-reorientation

Simulation models were conducted to find the optimal length of infill fractures. The models' fractures have no deflection at any angles (that is, no deflection, fractures parallel to the original direction of maximum principal stress N67°E). Figure 4 shows the results of optimal fracture length of infill wells at different locations. Well A is expected to have longer fracture half-length, the cumulative production oil improve with the increase of the fracture length. As fracture length increases around 70 m, the growth of cumulative production curve dives into the lower level. For well B, on the contrary, the maximum of cumulative production can be achieved when fracture half-length reach around 50 m. This confirms that the optimal value of infill fracture parameter is totally different

Table 1. Data for streamline simulation.

Reservoir size x-direction	520 m
Reservoir size y-direction	300 m
Reservoir pressure	9.13 MPa
Reservoir permeability	2.74×10^{-3} μm^2
Reservoir porosity	0.13
Pay thickness	11.4 m
Oil density	0.835×10^{3} kg/m^3
Viscosity	1.96×10^{-3} Pa·s
Formation volume factor	1.21
Primary hydraulic fracture length	120 m
Infill well fracture length	80 m
Hydraulic fracture conductivity	25 md·cm
Fracture aperture	0.03

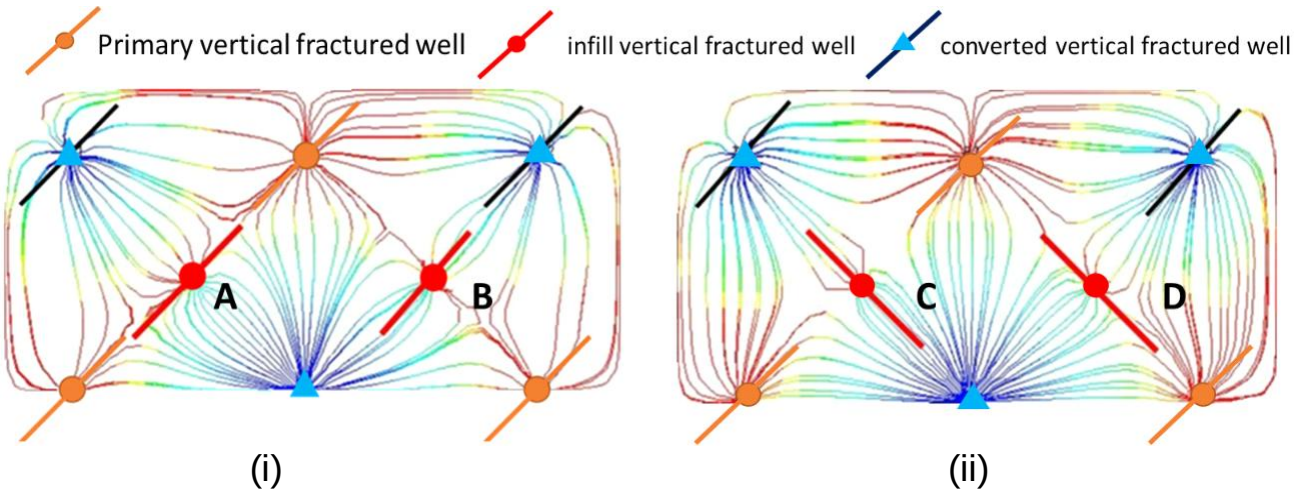

Figure 3. Infill well streamlines distribution with no deflection (0° angles; i); infill well streamlines distribution with 90°-deflected angles (ii). As the model is symmetrical (that is, mirroring the results), only half of the simulation is shown in the figures.

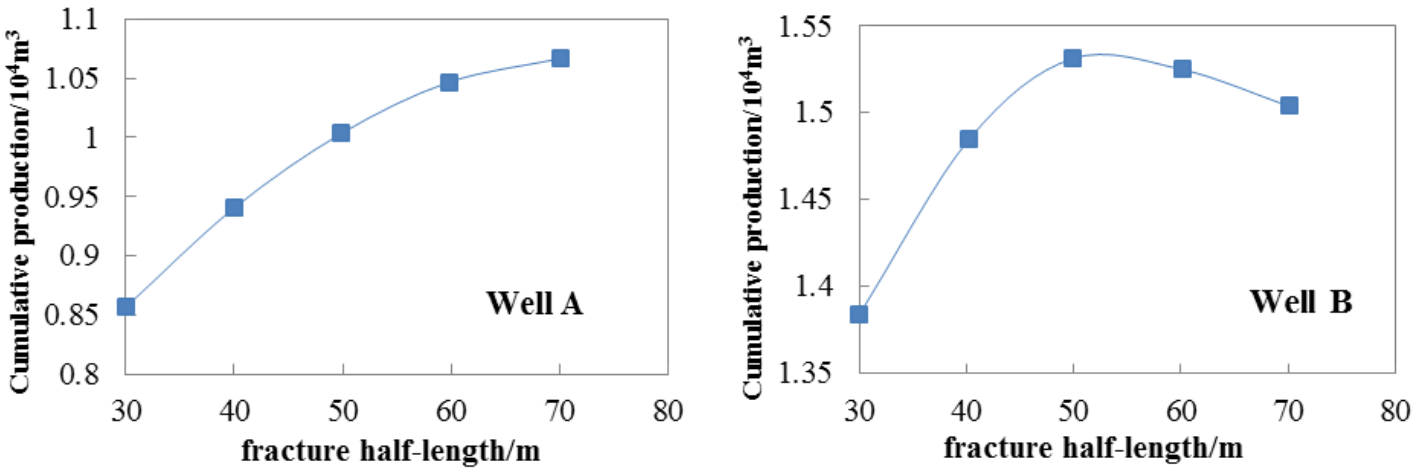

Figure 4. The curve of single well cumulative production versus fracture half-length (Infill well with no deflection)

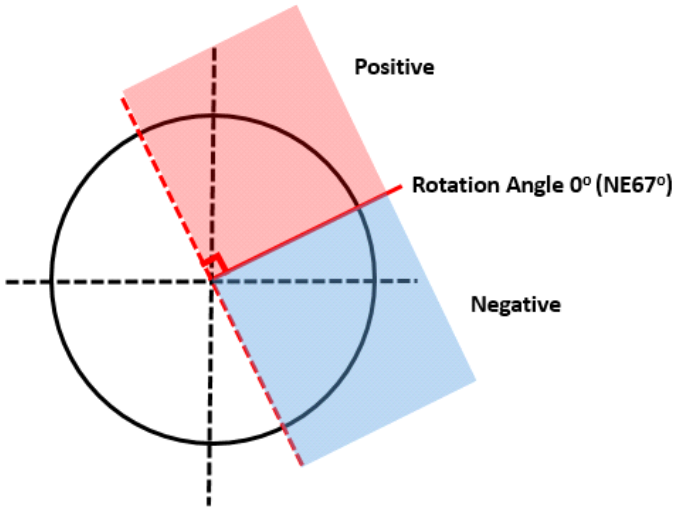

Figure 5. Scheme of the infill well fracture deflection angle.

in case of infill locations. In addition, the optimal result for infill Wells A and B can be affected by other factors, which primary fracture length and well space should be considered.

Cases with fracture reorientation

Assuming that infill fractures could reorient with arbitrary angle, in this case, 10 reservoir simulation models have been conducted to address the problem of optimal fracture length design with fracture reorientation. The original maximum stress direction (N67°E) was set as the initial value, which is zero rotation angle (θ = 0) (as shown in Figure 5). Infill fractures deflect in the circle to cover different areas, which anticlockwise the rotation angle increases. Otherwise, the angle decreases when the rotation is clockwise. Table 2 proposes the simulation schemes of different fracture deflection angles.

Figure 6 shows that the smaller deflection angles of the infill fracture can achieve, the more cumulative production. After 15 years' production, infill Well A at the angle ±33° always produced 30% more oil than at the rotation angle ±77°, which means that the smaller fractures' reorientation has benefit for ultimate reservoir recovery. Infill wells at different locations relative to injection wells have different optimal fracture length. For example, the optimal infill fracture length of Well B ranges from 50 to 60 m, which is smaller than Well A.

The summary of the optimal value of infill fractures with respect to the rotation angles is proposed in Figure 7. The solid line and the dashed line represent the optimal fracture half-length of Wells A and B with different relative locations, respectively. The optimal values of each well are symmetric about the maximum principle stress direction (θ = 0°). The entire range of angles can be divided into three regions: I, II and III.

In Region I, the optimal fracture half-length of Well B is longer than Well A. The optimal values keep constant with varying deflection angles in Region II; and in Region III, the relation between optimal infill fracture length of Wells A and B is opposite to that in Region I. The significant difference in the hydraulic fracture's length between Wells A and B is evident from simulation results and flow behavior, which is highly depended on infill fracture reorientation and the location of injection. However, the future fracture reorientation angles of infill wells are difficult to determine precisely in case of complex stress distribution in oil field with fractured well patterns especially after long-time production. If the infill fracture could not be optimized based on precise measurement of stress distribution, which is difficult to get actually, the water channeling would happen and lower the water flooding recovery. Obviously, it is meaningful to present MRO of infill fractures considering the balance between maximum production and safety risks.

Fracturing safety interval (FSI)

As previously mentioned, the understanding of infill well fracture propagation could be improved through the application of micro-seismic results as shown in Figure 2 into reservoir simulation analysis. Because most of micro-seismic results of infill wells (about 90%) as shown in Figure 2 show a rather small deflection angle between 0 and 60°, which means that greater probability of fracture reorientation are mostly likely to happen in Regions II and III (Figure 7). In this study, the weighting average method is employed to calculate the range of favorable fracture half-lengths considering the balance between maximum production and minmum risks due to fracture reorientation (Equation 1), which can also be called FSI.

Table 2. Simulation scheme of infill well fracture deflection angles.

Scheme	Rotation angle/°
1	23
2	-23
3	33
4	-33
5	47
6	-47
7	67
8	-67
9	77
10	-77

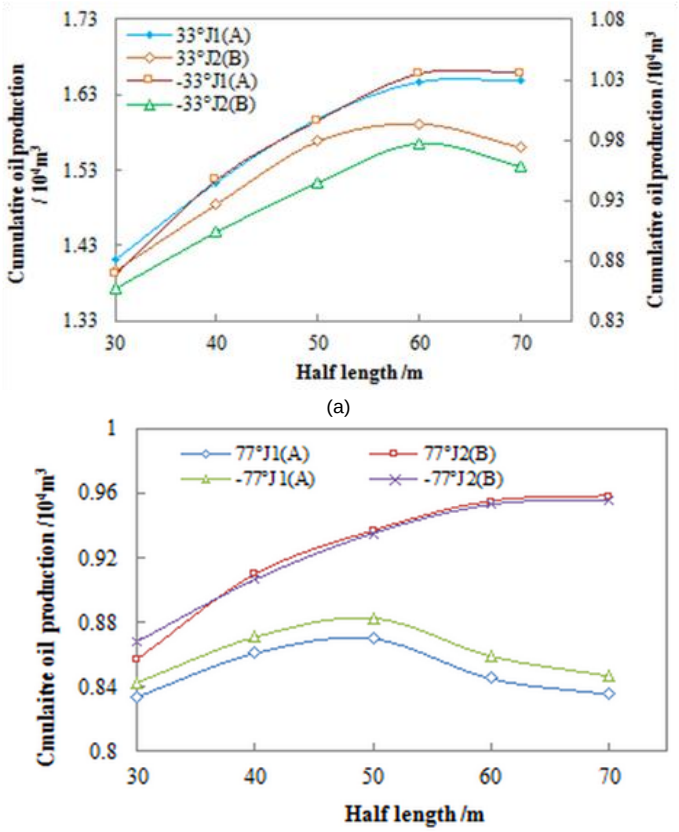

Figure 6. Cumulative oil production vs. rotation angles： (a) ±33° Rotation angle； (b) ±77° Rotation angle

$$FSI = \alpha(W_I L_I + W_{II} L_{II})/(W_I + W_{II}) \quad (1)$$

In Equation 1, *FSI* is the range of the favorable fracture half-lengths, W_I is the weight coefficient of Region I (percentage) and W_{II} is the weight coefficient of Region II (percentage), which is determined by the proportions of fracture reorientation in Regions I and II according to the statistics data of micro-seismic monitoring results (Figure 2). α is the safety factor, which we suggest to be ranged from 0.85 to 1.05 depending on the monitoring results of existing wells near infill well groups in study. The smaller the angle (0~90°) between the fracture orientation and production-injection connection line in the neighborhood well groups, the smaller this safety factor would be. L_I, L_{II}, the theoretically optimal fracture half-length depends on the values of different regions in Figure 7, for example, if fracture deflection angle in the neighborhood well groups was monitored to be larger than 60°, the recommended infill fracture half-length of well groups in study are around 60 m for both Group A wells B. So according to the fracture micro-seismic monitor data in the Ansai reservoir and simulation results discussed above, the approximate value of W_I, W_{II}, L_I, L_{II} can be assumed as shown in Table 3.

Thus, the FSI for Group A ranges from 54 to 64 m, and Group B ranges from 45 to 56 m. To test the result of well performance at the favorable fracture half-length determined by FSI, the favorable fracture half-length can be chosen for Group A (60 m) and Group B (50 m) which fracture deflection angle is 0°, 33° and 47°. As the fracture deflects to 67°, the optimal fracture half-length is same, which is both 60 m. The cumulative oil production result shows that under different fracture directions, well groups with favorable fracture half-lengths can always achieve a relatively good cumulative oil production (Figure 8). This proves that even if it is hard to determine the infill well fracture orientation, the fracture half-length still could be chosen from FSI (Table 4).

Conclusions

This study proposed one optimization approach for the fracturing design of infill wells in existing reverse nine-spot well patterns and its application in Ansai oilfield, CHN.

1) Infill well performance and micro-seismic monitoring results both show that the probability of fracture reorientation increase due to long-time production of existing well pattern. Some infill wells fractures show

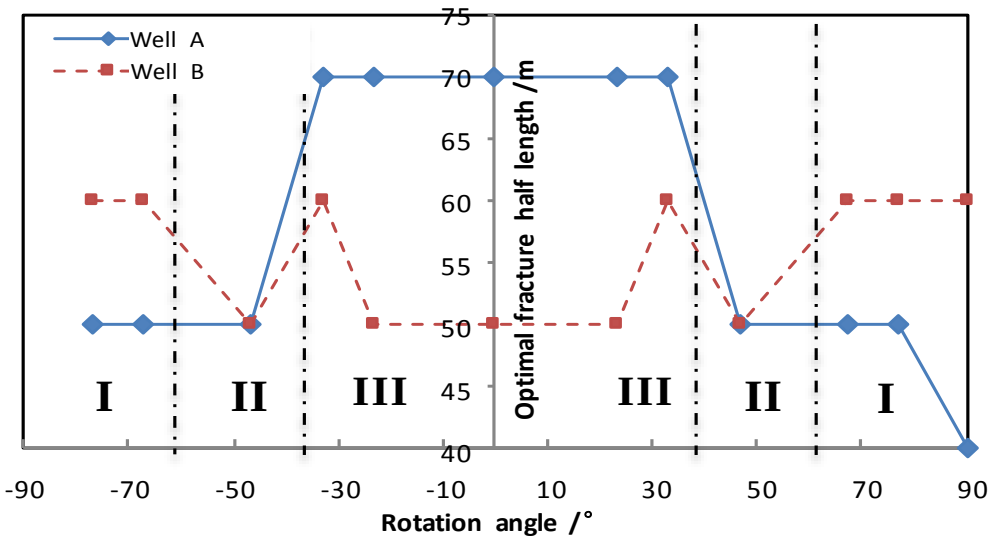

Figure 7. Optimal fracture length of Well A/B under different fracture reorientation angle and region division in Ansai low permeability oil reservoir.

Table 3. FSI calculations for infill wells.

Infill wells	Group A	Group B
W_I	60%	60%
W_{II}	30%	30%
L_I/m	70	55
L_{II}/m	50	50
α	0.85 - 1.00	

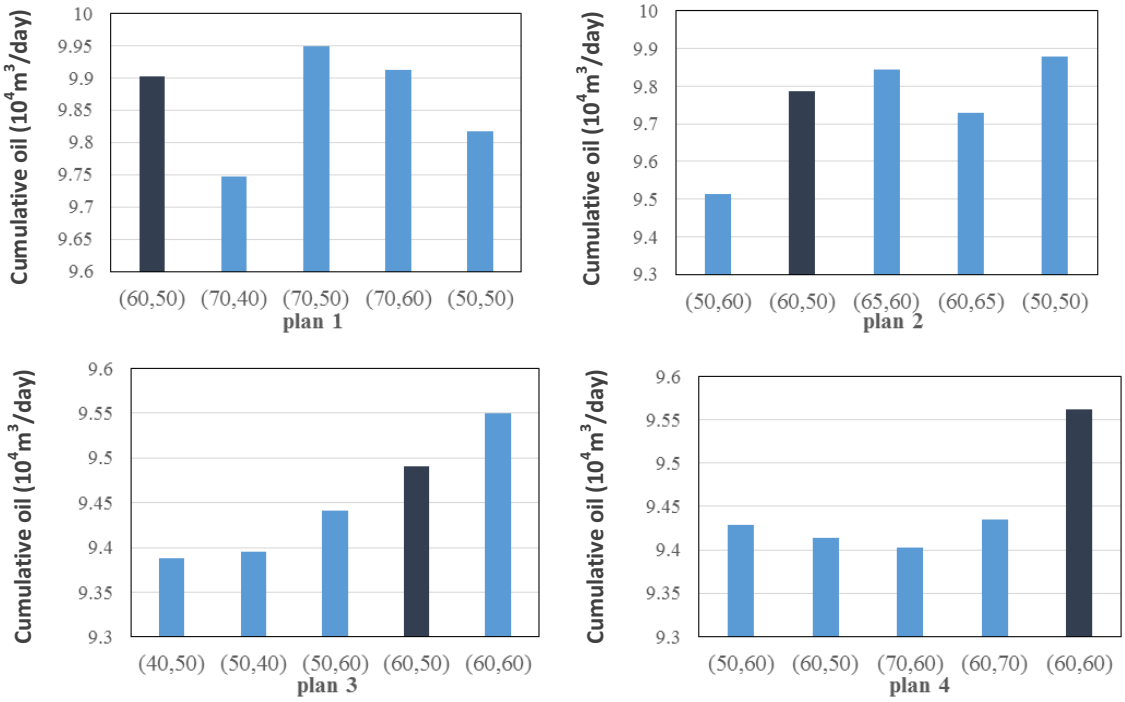

Figure 8. FSI test results for Ansai low permeability reservoir.

Table 4. FSI test schemes.

Schemes	Rotation angle/°	Fracture half-length (Well A, Well B)/m	FSI
1	0	**(60,50)** (70, 40) (70,50) (70,60) (50,50)	**(60,50)**
2	33	(50,60) **(60,50)** (65,60) (60,65) (60,60)	**(60,50)**
3	47	(40,50) (50, 40) (50,60) **(60,50)** (50,50)	**(60,50)**
4	67	(50,60) (60,50) (70,60) (60,70) **(60,60)**	**(60,60)**

adverse orientation, consequently causing serious consequences such as early water breakthrough, and even burst water floods, as happened to production wells in the pilot test.

2) Base on the well performance, infill wells in inverted nine-point pattern can be subdivided into two categories depending on their locations relative to existing injection wells. Wells of each group type have different optimal fracture half-lengths. However, they share one same optimal half-length within one same group.

3) According to the optimal fracture half-length under different fracture deflection conditions, three characteristics angle region have been identified. In Region I, the favorable fractures length of Well Group A should be larger that of Well Group B, and the opposite in region III, the approximately same in Region II.

4) Based on the difficulty of precise measurement of stress distribution after long-production in reservoirs, and the possible water channeling would happen after infill well fracturing. The MRO method and FSI are applicable to optimal design of infill fractures considering the balance between maximum production and uncertain safety risks.

Conflict of Interest

The author(s) have not declared any conflict of interest.

ACKNOWLEDGEMENTS

This paper was supported by Program for Changjiang Scholars and Innovative Research Team in University, PCSIRT (IRT1294); National Basic Research Program of China (2014CB239103), and The Fundamental Research Funds for the Central Universities (13CX06030A).

REFERENCES

Barber AH, George CJ, Stiles LH, Thompson BB (1983). Infill drilling to increase reserves-actual experience in nine fields in Texas, Oklahoma, and Illinois. SPE JPT. 35(08):1530-38.

Ching HW, Laughlin BA, Michel J (1989). Infill drilling enhances water-flood recovery. JPT 41(10):1088-95.

Deimbacher FX, Economides MJ, Jensen OK (1993). Generalized performance of hydraulic fractures with complex geometry intersecting horizontal wells. SPE Paper 25505 presented at the Production Operations Symposium held in Oklahoma City, Oklahoma. U.S.A. March 21-23.

Hidayati DT, Chen HY, Teufel LW (2001). Flow-induced stress orientation in a multiple-well reservoir. SPE Paper 71091 presented at the SPE Rocky Mountain Petroleum Technology Conference held in Keystone, Colorado, May 21-23.

Roussel NP, Horacio F, Adolfo AR (2013). Hydraulic fracture propagation from infill horizontal wells. SPE Paper 1666503 presented at SPE Annual Technical Conference and Exhibition, 30 September-2 October, New Orleans, Louisiana, USA..

Schutjens PM, Kuvshinov BN (2010). On the wellbore stress change caused by drawdown and depletion: an analytical model for a vertical well in a thin reservoir. SPE 136701, SPE Reserv. Eval. Engr. 13(04):688-698.

Rod HM (2005). Injection fracturing in a densely spaced line drive waterflood - The Halfdan Example." SPE Paper 94049 presented at the 2005 SPE Europe/EAGE Annual Conference held in Madrid, Spain, June 13-16.

Sharma A, Chen HY, Teufel LW (2008). Flow-induced stress distribution in a multi-well reservoir." SPE Paper 39914 presented at the 2008 Rocky Mountain Regional/Low Permeability Reservoirs Symposium and Exhibition held in Denver, Colorado, U.S.A, April 5-8.

Van Everdingen AF, Kriss HS (1980). A proposal to improve recovery efficiency. JPT 32(07):1164-1168.

Singh V, Roussel NP, Sharma MM (2008). Stress reorientation and fracture treatments in horizontal wells. SPE Paper 116092 presented at the SPE Annual Technical Conference and Exhibition, Denver, Colorado, USA, September 21-24.

Weijers L, Wright CA, Demetrius SL (1999). Fracture growth and reorientation in steam injection wells. SPE Paper 54079 presented at the 1999 SPE International Thermal Operations/Heavy Oil Symposium, Bakersfield, California, March 17-19.

Wright CA (1994). Reorientation of propped re-fracture treatments in the Lost Hills Field.SPE Paper 27896 at the 1994 SPE Western Regional Meeting, Long Beach, California, March 23-25.

Wright CA, Conant RA (1995). Hydraulic fracture reorientation in primary and secondary recovery from low-permeability reservoirs. SPE Paper 30484 at the SPE Annual Technical Conference and Exhibition, Dallas, Texas, October 22-25.

Wolhart SL, McIntosh GE, Zoll MB, Weijers L (2007). Surface tiltmeter mapping shows hydraulic fracture reorientation in the Codell Formation. SPE Paper 110034 at the SPE Annual Technical Conference and Exhibition, Anaheim, California, U.S.A. November, 11-14.

Zhai ZY, Sharma MM (2007). Estimating fracture reorientation due to Long Term Fluid injection/production." SPE Paper 106387 presented at the 2007 SPE Production and Operations Symposium held in Oklahoma City, Oklahoma, U.S.A, March 31- April 3.

academicJournals

Vol. 5(5), pp. 57-69, November, 2014
DOI: 10.5897/JPGE2014.0203
Article Number: FA5E23548321
ISSN 2141-2677

http://www.academicjournals.org/JPGE

Journal of Petroleum and Gas Engineering

Full Length Research Paper

A practical approach to the evaluation of subcritical multiphase flow through down-hole safety valves (storm chokes)

A. Joseph* and J. A. Ajienka

Department of Petroleum and Gas Engineering, University of Port Harcourt, Nigeria.

Received 12 August, 2014; Accepted 10 October, 2014

A practical approach to the evaluation of subcritical multiphase flow through down-hole safety valves (storm chokes) is presented. This method which is independent of the continuous phase is based on the composition of the flowing mixture and the operating temperature and pressure. In the event of single phase flow, the method can also be applied. With this method, we can easily size subsurface safety valves (SSSV) and chokes as well as determine pressure drops and flow capacities in them. The procedure for the use of this method is outlined and examples illustrate its applicability.

Key words: Multiphase flow, safety valves, down-hole, pressure drops.

INTRODUCTION

Multiphase flow through pipes is an aspect of study that investigates the concurrent flow of different phases such gas, liquid and solids in a pipe. It has several applications in different industries based on the peculiarities of different flow regimes associated with flow phases in different geometries and configurations of a piping system. Examples of such industries include: the nuclear industry where extensive work has been done to investigate critical heat flux, entrainment and deposition occurring in reactors (Stevanovic and Studovic, 1995; Alipchenkov et al., 2004; Pan and Hanratty, 2001; Kataoka et al., 2000); in the chemical industry where it could be used to investigate the interaction of deformable bodies (De Rosis, 2014), phase-separating flows at large density ratios (Falcucci et al., 2010) and harmonic oscillations of laminae in non-Newtonian fluids (De Rosis, 2014). It is also used in naval engineering to investigate the impact between sea waves and ship hulls which may generate impulsive forces that are strictly related to water splash-ups and air trapping (Takagi and Dobashi, 2003; Quin and Batra, 2009). In the petroleum industry, multiphase flow is most often used to investigate phase interactions and hydrocarbon accounting.

FLOW THROUGH RESTRICTIONS

The use of subsurface safety valves (SSSV) and storm chokes is one of the most important current applications of flow through deliberate restrictions in the oil and gas industry. The application is governed by subcritical flow theory. Subcritical flow is the flow during which any

*Corresponding author. E-mail: vonkarma@yahoo.com.

downstream flow perturbation is transmitted upstream of the restriction and influences the flow rate; that is, the fluid velocity through the choke will be less than the local velocity of sound (Binder, 1955; Nind, 1981). Flow is critical when fluid velocity is identical to the local velocity of sound in the fluid and downstream perturbations are no longer transmitted in the upstream direction. Critical flow conditions are desirable in surface flow operations. Most flowing wells flow from a condition of subcritical flow to that of critical flow at the wellhead. Thus, an accurate evaluation of the performance of sub-surface chokes is of great importance as it has a great impact on the performance of wellhead chokes which are used (Brown, 1984) for the maintenance of correct well allowable, maintenance of sufficient back pressure to prevent sand entry, protection of surface equipment, prevention of gas and water coning, and production of the reservoir at the most efficient rate.

The installation of SSSV or storm chokes in producing wells is required by law. These valves are normally installed on a "fully open" status. In the unfortunate event of damage to wellhead or tubing, to avoid wastage and spillage, these valves are automatically actuated to close. They can be surface controlled or actuated by velocity or temperature pre-setting. Figure 1 shows three common types of them used in the industry. Subsurface chokes can be used to cause an increase in velocity of fluid in the tubing and thus increase the gas lifting capacity of oil by causing the release and expansion of solution gas (Ros, 1961). Ros (1961) noted that for wells of low energy or velocity, we can achieve steadier flow, prolonged flowing life and in some cases reduction in gas-oil ratio (GOR), water-oil ratio (WOR) and an increased rate of production.

There are cases where excessive surface choking could lead to liquid loading and killing of well. Ross (1932) also reported cases where bottom hole choking of high pressure gas wells led to the advantage of higher and more uniform underground temperature, thus reducing freezing at the surface during winter and permits more efficient water removal.

Although the most efficient results could be obtained by choking at the bottom of the tubing; Ross (1932) suggested that in wells with high fluid levels, it may be desirable to choke just below the fluid working level and successively lowering the choke level as fluid recedes. This initial critical point in the tubing should be determined from a series of tests.

Previous works

It is known that the prediction of subcritical flow behavior is far more difficult than critical flow and very little work has been done for subcritical flow (Al-Attar, 2009). Nevertheless, for a given flowing mixture and operating conditions, the accurate delineation of the subcritical flow region is dependent on the ability to correctly predict when critical flow actually occurs. Olson (1980) emphasized that the conditions for critical or subcritical single phase flow do not apply to multiphase flow. Most researchers (Ashford, 1974; Beggs and Brill, 1984; Gilbert, 1954; Poetmann and Beck, 1963; Ros, 1961) have assumed that for single phase flow, the critical multiphase flow occurs at a fixed pressure ratio, X_c, irrespective of the flowing mixture and operating temperature and pressure. Because of such self imposed limitations, it is unsafe to assume that subcritical multiphase flow occurs at pressure ratios greater than the fixed critical pressure ratio.

Ajienka and Ikoku (1987) presented a simple method for predicting critical multiphase flow which is dynamic, as it is dependent on the composition of the flowing mixture and operating conditions. The study was also confirmed by observations made by Olson (1961) and Fortunati (1972) that the critical pressure ratio for multiphase flow can be as low as 0.225 and as high as 0.60 depending on the composition of the mixture and operating temperature and pressure. Again, it can easily be observed that most multiphase orifice correlations for critical or subcritical flow implicitly assume continuous liquid phase flow and so cannot be used for a condition of continuous gas phase flow such as mist flow encountered in condensate production.

Guo et al. (2007) evaluated the accuracy of the Sachdeva et al. (1986) multiphase choke flow model using data from 239 oil wells and 273 gas condensate wells in Southwest Louisiana. They made comparisons of their results and found that Sachdeva et al. (1986) model is more accurate for oil wells than gas condensate wells and the choice of the value of discharge coefficient used in the model has significant effect on the accuracy and error margins observable. Elgibaly and Nashawi (1998) developed a simple empirical correlation for Middle East data through the investigation of the effects of coupling the Ashford and Pierce (1975) multiphase flow correlation using newly developed pressure-volume-temperature (PVT) correlation for Middle East crudes. They observed that the use of the regional PVT correlations significantly improved the prediction of the Ashford and Pierce (1975) model.

Beggs and Brill (1984) reported that until recently, safety valves were normally sized on the basis of single phase liquid flow calculations and that this technique has been found to be highly questionable. Ross (1936) even reported that in high GOR wells, sizing was based on gas equations, with allowance made for oil production and solution gas at the operating pressure. He further reported that estimating the proper size of the bean in low GOR wells was more difficulty and the correct size was usually determined by trial and error and that from experience the size of the bottom hole choke is considerably smaller than the surface choke for a given rate of production.

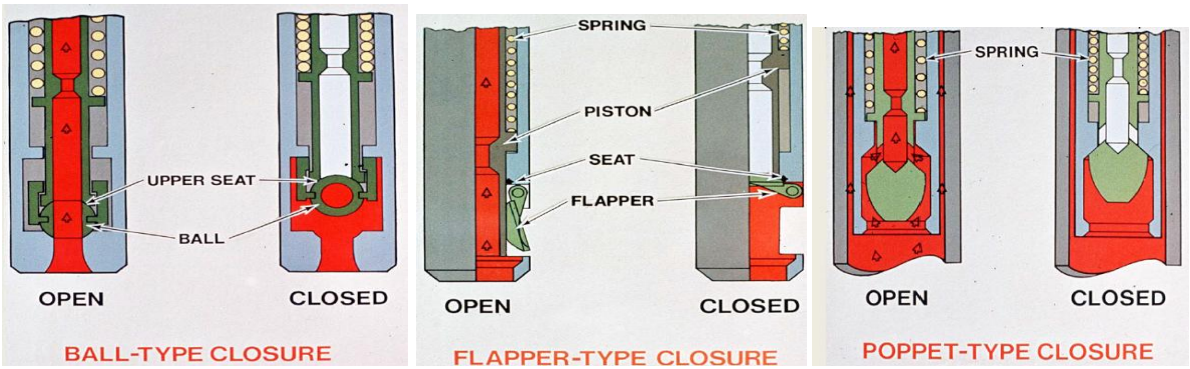

Figure 1. Types of storm chokes used in the industry.
http://gekengineering.com/Downloads/Free_Downloads/Subsurface_Safety_Valve_Basics.pd

Based on a combination of Bernoulli's equation with an equation of continuity, the subcritical flow rate in (ft^3/s) for liquids is given by Beggs and Brill (1984):

$$q = CA_0\left(\frac{2g_c(144)\Delta P}{\rho}\right)^{\frac{1}{2}} \quad (1)$$

Where C is the discharge coefficient, A_0 is the area of the restriction, g_c conversion factor for acceleration due to gravity, 32.17 $lbft/s^2$, ρ is the density of the oil and ΔP is the drop across the choke.

Equation 1 can be solved to evaluate the pressure drop across the choke or the choke size. The flow coefficient is a function of the meter, the diameter ratio between choke and pipe, the approach velocity factor, the Reynolds number and the position of the vena contracta for the orifice. Assuming a steady-state isentropic flow, Equation 1 is multiplied by an expansion factor (Y) to give the subcritical flowrate for gases.

$$Y = 1.0 - \left[0.41 + 0.35\left(\frac{d}{D}\right)^4\right]\left(\frac{1}{K}\right)\left(\frac{\Delta P}{P_1}\right) \quad (2)$$

This accounts for the compressibility effect.

As has been observed, it is unsatisfactory to use the above equations and estimation methods to evaluate subcritical multiphase flow because it was developed on the assumption of no-slip single phase flow and thus devoid of factors that account for gas solubility, the WOR, liquid-gas ratio etc that is representative of typical multiphase flow models. Unfortunately, very few papers have been presented on the evaluation of subcritical multiphase flow in the industry.

By assuming a no-slip mixture density, isentropic flow, a mass ratio based polytropic exponent, no-mass transfer between the phases and physical properties calculated at downstream conditions, Fortunati (1972) proposed Equation 3 for predicting liquid flowrate:

Liquid rate = Cross-sectional area × velocity

$$q_o = \frac{A_c(1-\lambda_g)}{B_o}C_D V' = \frac{A_c(1-\lambda_g)}{B_o}C_D V\left(\frac{P_2'}{P_2}\right)^{\frac{\eta}{2}} \quad (3)$$

Where

$$\eta = \left(1-\lambda_g^3\right)^{0.38} \quad (4)$$

$$\lambda_g = \frac{q_g}{q_g + q_o}$$

and q_o is liquid rate m^3/s, A_c is the total choke cross-sectional area, m^2, λ_g is the gas concentration with respect to the total mixture, C_D is the discharge coefficient, P_2' is the actual choke downstream pressure, MN/m^2, P_2 is the choke downstream pressure, 0.137 MN/m^2, and V is the mixture velocity corresponding to the downstream pressure P_2, m/s,

Fortunati (1972) stated that the critical pressure ratio is a function of the no-slip liquid holdup, λ_L. A major limitation is that it is prepared for downstream pressure of approximately 20 psia.

To correct the mixture velocity for actual downstream

pressure, the following expression is used:

$$V^{'} = V\left(\frac{P_2^{'}}{P_2}\right)^{\frac{\eta}{2}} \quad (5)$$

Extending the work of Ros (1961), Ashford and Pierce (1975) presented a relationship for two-phase subcritical flow given as:

$$q_0 = 3.51 C_D d^2 \alpha_{10} \beta_{10}$$

Where:

$$\alpha_{10} = \left(B_0 + F_w\right)^{-1/2}$$

and

$$\beta_{10} = \frac{\left[\left(\frac{1}{b}\right) T_1 z_1 \left(R - R_s\right)\left(1 - X^b\right) + 198.6 p_1 \left(1 - X\right)\right]}{\left[198.6 + \frac{T_1 z_1}{p_1}\left(R - R_s\right) X^{\frac{-1}{n}}\right]} \times \frac{\left[\left(\gamma_o + 0.00217\gamma_o R_s + F_w \gamma_w\right)\right]^{\frac{1}{2}}}{\left(\gamma_o + 0.00217\gamma_o R_s + F_w \gamma_w\right)} \quad (6)$$

Where: R **,** Producing GOR; R_s **,** solution gas oil ratio; **b,** $(n-1)/n$; **n,** specific heat ratio, c_p / c_v; **X,** the pressure ratio, p_2 / p_1 ; p_1 **,** upstream orifice pressure, psf; p_2 **,** downstream orifice pressure, psf; C_D **,** the discharge coefficient; **d,** the choke diameter; γ_o **,** oil gravity; γ_w , water gravity; F_w , water oil ratio (WOR); T_1 , upstream orifice temperature; z_1 , gas compressibility factor at T_1 and p_1 ; q_0 **,** oil rate, B/D; B_0 **,** formation volume factor.

In their correlation, Ashford and Pierce (1975) assumed that the gas flowing through the choke expanded polytropically, mixture flow through choke is isentropic (frictionless and adiabatic), no slippage between the phases and an incompressible continuous liquid phase. Iterating on Equation 6, they obtained a subcritical pressure ratio:

$$X_c = \frac{\frac{R_1}{n}\left[\frac{R_1 n}{n-1}\left(1 - X_{est}^{(n-1)/n}\right) + \left(1 - X_{est}\right)\right]}{0.5\left[1 + R_1 X_{est}^{-1/n}\right]^2 X_{est}^{(n+1)/n}} \quad (7)$$

Where:

$$R_1 = \frac{p_{sc} T_1 z_1}{p_1 T_{sc}}\left(R - R_s\right)\frac{1}{5.615}$$

X_c is the subcritical pressure ratio and X_{est} is the estimated pressure ratio, T_{sc} is the atmospheric temperature, p_{sc} atmospheric pressure, R is the producing GOR and R_s is the solution GOR.

Equation 7 normally has two roots, one less than X_c and one greater than X_c. It is also possible that the condition may arise where one or no possible root can be found. Even though their work covered 20/64th inch choke size, they recommended different orifice discharge coefficients, C_D, for different choke sizes (Table 1). Also, their plot assumes that subcritical flow must occur at X > 0.5.

Beggs and Brill (1984) reported other models for evaluating subsurface controlled SSSV such as the API 14B Model and the University of Tulsa Model. The API 14B is a computer program developed to size SSSV. Assumptions made in the formulation are as follows:

a) Liquid flow through the choke is incompressible. The discharge coefficient, C_D is constant with a default value of 0.85.
b) Subcritical gas flow through choke is adiabatic and compressible. The C_D is constant with a default value of 0.90.
c) Subcritical two-phase compressible flow is described by weighting the liquid and gas orifice flow equations with the no-slip fraction of free gas (g) in the stream, approaching the choke.
d) The density and flow rate of each phase can be replaced by a no-slip mixture density, ρ_n and a total mixture flow rate, q_m.

Combining Bernoulli's equation with the continuity equation, they obtained an equation for incompressible flow through an orifice or nozzle as:

$$q_m = \frac{C_D A_B \left(\frac{2\Delta P_{TP}}{\rho}\right)^{\frac{1}{2}}}{\left[1 - \left(\frac{dB}{dt}\right)^4\right]^{\frac{1}{2}}} \quad (8)$$

The two-phase pressure drop is defined as:

$$\Delta P_{TP} = \Delta P_L \lambda_L + \Delta P_g \lambda_g \quad (9)$$

By using the expansion factor Y of Equation 2, in combination with the above equations and applying the appropriate conversion factors, Equation 9 was transformed to:

$$\Delta P_{TP} = \Delta P_L \left\{1 - \lambda_g \left[\left(\frac{C_{DL}}{Y C_{Dg}}\right)^2 - 1\right]\right\} \quad (10)$$

Table 1. Ashford and Pierce (1975) C_D recommendations.

Choke size (64th inch)	C_D
32	0.95
24	0.95
20	0.9760
12	1.2
8	1.2

Where ΔP_L and ΔP_g are the pressure drops due to the liquid and the gaseous phases, C_{DL} and C_{DL} are the discharge coefficients of the liquid and vapor phases, λ_L and λ_g are the non-slip liquid and gas holdups.

The University of Tulsa Model is a homogenous model for predicting pressure drop across two specific velocity controlled SSSV, the 2-inch Otis J and Camco A-3 valves. The two-phase pressure drop is calculated as:

$$\Delta P_{TP} = \frac{\rho_n V_{mB}^2}{2 g_c C_D^2} \tag{11}$$

Where: ρ_n is the non-slip density, V_{mB} is the mixture velocity and C_D is the discharge coefficient. The non-slip density, ρ_n , V_{mB} and C_D are evaluated at upstream pressure and temperature. Using experimental data an empirical discharge coefficient correlation for each valve was proposed as:

$$C_D = C_0 + C_1 RD + C_2 RD2 + C_3 VD \tag{12}$$

$$RD = \frac{d_B}{d_t} \tag{13}$$

$$VD = \frac{V_{sg}}{V_{sL}} = LGR1 \tag{14}$$

C_i = empirical coefficients given in Table 2.

Apart from the API 14B and the University of Tulsa Models, the others are analytical subcritical flow correlations which differ essentially in the definition of subcritical flow, range and method of application as well as the fact that they can only be applied to continuous liquid phase flow and do not reduce to single phase relationships.

Ajienka (1985) and Ajienka and Ikoku (1987) also presented a generalized analytical multiphase orifice flow equation valid for both continuous liquid phase flow and continuous gas phase flow and is flexible enough to be used for their critical and subcritical flow. This relationship yields the familiar phase orifice flow equations in the limit of single phase flow. The relationship has been validated with reported field data. There are also ongoing new methods of predicting critical flow and thus delineating the subcritical flow region has been reported.

PROPOSED PRACTICAL APPROACH

Assuming the homogenous flow model similar to Ashford and Pierce (1975), the generalized multiphase orifice flow model was grouped into factors as:

$$q_{TP} = f_b \beta R_{mp} F\left(\frac{P_2}{P_1}\right) \tag{15}$$

Where f_b is the base factor, β is the beta factor, R_{mp} is the multiphase specific volume factor and $F\left(P_2 / P_1\right)$ is the dimensionless pressure function, P_1 and P_2 are the upstream and downstream pressures of the choke respectively.

Note that depending on the continuous phase, we can apply phase correction factors (Ajienka, 1984) to reduce Equation 15 to wanted single phase flowrates. The only term in Equation 15 which incorporates pressure ratio, X, is the dimensionless pressure function.

$$F\left(\frac{P_2}{P_1}\right) = F\left(X\right)$$

Assuming polytropic flow of the gaseous phase,

$$F\left(X\right)_{mp} = \frac{[LGR_1(1-X) + \frac{1}{b}(1-X^b)]^{\frac{1}{2}}}{[LGR_1 + X^{-1/k}]} \tag{16}$$

Where:

$$LGR1 = \frac{198.413 P_1 (Bo + WOR)_1}{Z_1 T_1 (R - Rs)_1} \tag{17}$$

X is the pressure ratio, b = $(n-1)/n$, n = C_p / C_v, B_o is the oil formation volume factor, Z_1 is the gas compressibility factor

Table 2. Empirical coefficients for orifice discharge correlation (Beggs and Brill, 1984).

Coefficient	Camco liquid	Camco two-phase	Otis liquid	Otis two-phase
C_0	0.2815	0.5417	1.8247	1.1819
C_1	9.4691	3.8749	-13.9697	-1.8761
C_2	-25.5689	-10.4536	51.0889	0.9922
C_3	0	0	0	-0.0119

calculated at P_1 and T_1, WOR is the water-oil ratio.

LGR1 is the dimensionless liquid-gas-ratio at upstream of choke conditions expressed in terms of the PVT properties of the mixture. For the special case of isothermal compressible flow, the dimensionless pressure function was derived as:

$$F\left(X\right)_{mi} = \frac{[LGR_1(1-X)-\ln X]^{\frac{1}{2}}}{[LGR_1 + X^{-1}]} \quad (18)$$

The other factors which are independent of X are defined as:

Base factor

$$f_b = 1.970 C_D d_c^2; \quad (19)$$

Multiphase Beta factor

$$\beta = p_1^{0.5}\left[\frac{2.7026\gamma_g p_1}{Z_1T_1} + \left(62.4\left(\gamma_o + WOR\right) + 0.01353\gamma_g R_s\right)\left(\frac{198.413 p_1}{Z_1T_1(R_p - R_s)}\right)\right]^{0.5} \quad (20)$$

Multiphase specific volume factor

$$R_{mp} = \frac{\left(Bo + WOR\right) + 0.00504 Z_1T_1(R_1 - R_s)/P_1}{62.4(\gamma_o B_o + WOR) + 0.0135\gamma_g R_1}, \quad (21)$$

Where: C_d is the discharge coefficient, d_c is the choke diameter,

Iterating on Equations 16 and 18, we can obtain expressions for the subcritical pressure ratio (for $X_{est} > X_c$) as:

$$X_{sc} = \left[\left(\frac{LGR_1\left(1-X_{est}\right) + \frac{1}{b}\left(1-X_{est}^{b}\right)}{F\left(X_{est}\right)_{mp}^2}\right)^{\frac{1}{2}} - LGR_1\right]^n \quad (22)$$

For isothermal flow, the subcritical pressure ratio becomes:

$$X_{sc} = \left\{\left[\frac{LGR_1(1-X_{est}-\ln X_{est}}{F\left(X_{est}\right)_{mi}^2}\right]^{\frac{1}{2}} - LGR_1\right\}^{-1} \quad (23)$$

Note that Equation 22 is similar to Equation 7 by Ashford and Pierce (1975). Also, note that the value of X_{sc} is very sensitive to $F(X_{est})$. Thus, for subcritical multiphase flow using the predicted X_{sc}, the flowrate is given as:

$$q_{TP} = F_b \beta R_{mp} F_{mp}\left(X_{sc}\right) \quad (24)$$

If oil is the wanted continuous flow rate, then

$$q_o = q_{TP} F_{mp} \quad (25)$$

Where:

$$F_b = 1.97 C d^2 \quad (26)$$

Multiphase Beta factor is defined as:

$$\beta = p_1^{0.5}\left[\frac{2.7026\gamma_g p_1}{Z_1T_1} + \left(62.4\left(\gamma_o + WOR\right) + 0.01353\gamma_g R_s\right)\left(\frac{198.413 p_1}{Z_1T_1(R_p - R_s)}\right)\right]^{0.5}$$

Multiphase specific volume factor

$$R_{mp} = \frac{B_o + WOR + A}{C + D} \quad (27)$$

$$A = 0.00504 T_1 Z_1 (R_p - R_s) / p_1 \quad (28)$$

$$C = 62.4\left(\gamma_o B_o + WOR\right) \quad (29)$$

$$D = 0.01353\gamma_g R_p \quad (30)$$

Dimensionless pressure factor is given as:

$$F_{mp}\left(X\right) = \frac{\left[LGR_1\left(1-X\right) + \frac{k}{\left(k-1\right)}\left(1-X\right)^{\frac{k-1}{k}}\right]}{LGR_1 + X^{\frac{-1}{k}}} \quad (31)$$

$$LGR_1 = \frac{198.413 p_1 (B_o + WOR)}{Z_1 T_1 (R_p - R_s)} \quad (32)$$

Multiphase correction factor for oil rate

$$F_{mp} = \frac{B_o}{B_o + WOR + \dfrac{0.00504 Z_1 T_1 (R_p - R_s)}{p_1 (B_o + WOR)}} \quad (33)$$

The wetness correction factor (F_W) for calculating gas rate is determined with the equation:

$$q_g = q_{Tp} . F_w \quad (34)$$

$$F_w = \frac{1}{1 + LGR_1} \quad (35)$$

Where Otis and Camco Valves are used, Equation 12 can be used to predict C_D in Equation 19.

METHOD OF STUDY

To ease the tedium of iteration and avoid the possibility of using incorrect X, the simple graphical approach for predicting and delineating the subcritical flow region is used. Also, each of the factors in Equation 24 has been graphed for added flexibility of use. However, we can also incorporate all the factors to graphically predict q for given conditions of flow.

It is possible to measure the pressure (P_2) just above the valve (downstream) of flow. In such a case, P_1 in our equations can easily be predicted as function of P_2 and pressure drop ΔP . Note that:

$$\Delta P = P_1 (1 - X_{sc}) = P_2 \left(X_{sc}^{-1} - 1 \right) \quad (36)$$

It can be added that to determine pressure drop or size of valves we can use reservoir flow rate as q_{TP} . P_1 can be estimated from vertical multiphase flow correlations (Beggs and Brill, 1984).

RESULTS AND DISCUSSION

It can be observed in Equations 16 and 18 and Figure 6 that for low P_1 and R, the difference between $F(X_{sc})_{mp}$ and $F(X_{sc})_{mi}$ is negligible. However, in most cases and for higher P_1 and R, $F(X_{sc})_{mp}$ is greater than $F(X_{sc})_{mi}$, thus, subcritical multiphase flow rate assuming polytropic expansion of the gaseous phase is slightly greater than the rate for isothermal expansion of the gaseous phase. The reverse is true for ΔP considering either polytropic or isothermal expansion of the gaseous phase. The effect on the size of the choke follows the same trend as ΔP.

The cross-plot of Figure 7 makes a comparison between some of the existing sub-critical multiphase correlations with our model. The diagonal line is the actual solution, while the data points are the predicted multiphase flowrates. All data points on the line predicts the actual rate correctly, those above the line over-predicts it while those below it under-predict the multiphase flow rate. As can be seen in Figure 7 along with the error analysis of Table 3, our model show little disparity with other models and predicted the actual rates better than others in three of the cases investigated. The disparity could be adjudged to be governing principle behind the derivation of the various models and the data integrity used in this comparison.

FIELD APPLICATION

General procedure

i. For any given field, use the relevant PVT data and the appropriate dimensionless pressure function to generate plots of F(X) versus X using average values of LGR1 for various values of P1. A simple program can be written to accomplish this task.
ii. For subcritical flow calculation, use the range $X_{sc} > X_c$ (predicted)
iii. Obtain X_{sc} and the corresponding $F(X_{sc})$.

Specific procedures and examples

1) Calculate multiphase flow capacity

Given the fluid characteristics, PVT data, choke size and operating pressure and temperature

i) Determine X_c
ii) Knowing P_1 or P_2 estimate ΔP from experience and then from Equation 26. Estimate if:

$X_{est} > X_c$, then $X_{est} = \dfrac{P_2}{P_1} = \left(1 - \dfrac{\Delta P}{P_1}\right) = \left(\dfrac{\Delta P}{P_2} + 1\right)^{-1}$

iii) Obtain $F(X_{est})$
iv) Calculate X_{sc} from Equation 22 or 23
v) If $X_{sc} > X_c$ and for high speed computation, check convergence: $|X_{est} - X_{sc}| \leq 0.001$, then use predicted X_{sc}.
vi) If not use $X_{sc} = X_{est}$
vii) Go back to set p in step (ii) and continue until convergence is achieved
viii) Finally obtain $F(X_{sc})$ from the Figures 6(a or b)
ix) Calculate f_b, β and R_{mp}.
x) Calculate multiphase flow capacity q_{TP} (Equation 24)
xi) If continuous phase flow capacity is desired correct q_{TP} for entrained phase(s).
xii) If q_o is not close to well test and manufacturers data

Table 3. Error analysis.

Method	Ashford and Pierce	Ajienka	Sachdeva	Tulsa/API
AAE%	17.8	15.5	16.2	40.7
CDavg.	1.19	0.98	0.90	1.6

Where AAE is the average absolute error and CD is the discharge coefficient.

go back to step (ii).

Example 1: Given the following, predict the multiphase flow capacity.

K	=	1.04	T_1	=	560°R-580°R (range)
Bo	=	1.01 bbl/STB	WOR	=	0.0
r_g	=	0.95	Rs	=	0.0 SCF/STB
r_o	=	0.885	R_1	=	500 SCF/STB
P_1	=	25000 psia	C_D	=	0.95
dc	=	16/64th			

Solution: (a) Assuming P_2 = 2000 psia, then

$$\frac{P_2}{P_1} = \frac{2000}{2500} = 0.8 = X_{sc}$$

$F(0.8)_{mp}$ =	0.21	(Figure 6a)	
f_b	=	479	(Figure 2)
β	=	680	(Figure 3)
R_{mp}	=	0.023	(Figure 4)

From Equation 24

$$q_{TP} = F_b \beta R_{mp} F(X_{sc})$$
$$q_{TP} = (479)(680)(0.023)(0.21)$$
$$q_{TP} = 1573.23 BPD$$

From Equation (25)

$$q_o = q_{TP} F_{mp}$$

F_{mp}	=	0.68(Figure 5)
q_o	=	(1573.23)(0.68)
q_o	=	<u>1070 BOPD</u>

(b) Assuming P_2 was not known then we iterate on X_{sc}.

Solution: From Figure (6a) X_c = 0.46

Assuming ΔP = 400 psia

$$X_{est} = \frac{P_2}{P_1} = \left(1 - \frac{\Delta P}{P_1}\right)$$

$$X_{est} = \left(1 - \frac{400}{2500}\right) = 0.84 > X_c$$

$$q_{TP} = 1610.7 BPD$$

$$F(X_{est}) = 0.22$$

$$X_{sc} = 0.85$$

$$F(X_{est}) = 0.215$$

$$q_{TP} = (479)(680)(0.023)(0.215)$$

$$q_{TP} = 1610.7 BPD$$

$$q_o = q_{TP} F_{mp} = 1610.7 * 0.68 = 1095 BOPD$$

2) Calculate pressure drop

Knowing the flow rate, flowing fluid characteristics and P_1 or P_2

1. Calculate fb, β and Rmp.
ii. From Equation 24,

$$F(X_{sc}) = \frac{q_{TP}}{f_b \beta R_{mp}} \quad (37)$$

iii. Using $F(X_{sc})$ in (ii) above and the appropriate dimensionless pressure function plot, determine the corresponding X_{sc} and check if $X_{sc} > X_c$.or if you use a program predict the

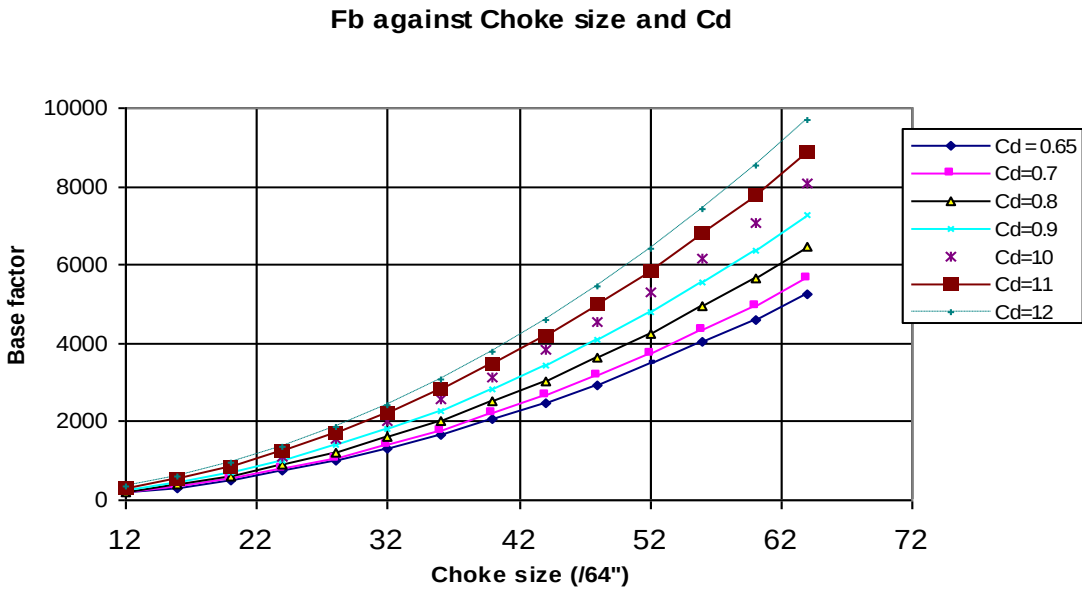

Figure 2. Base factor for estimating choke sizes.

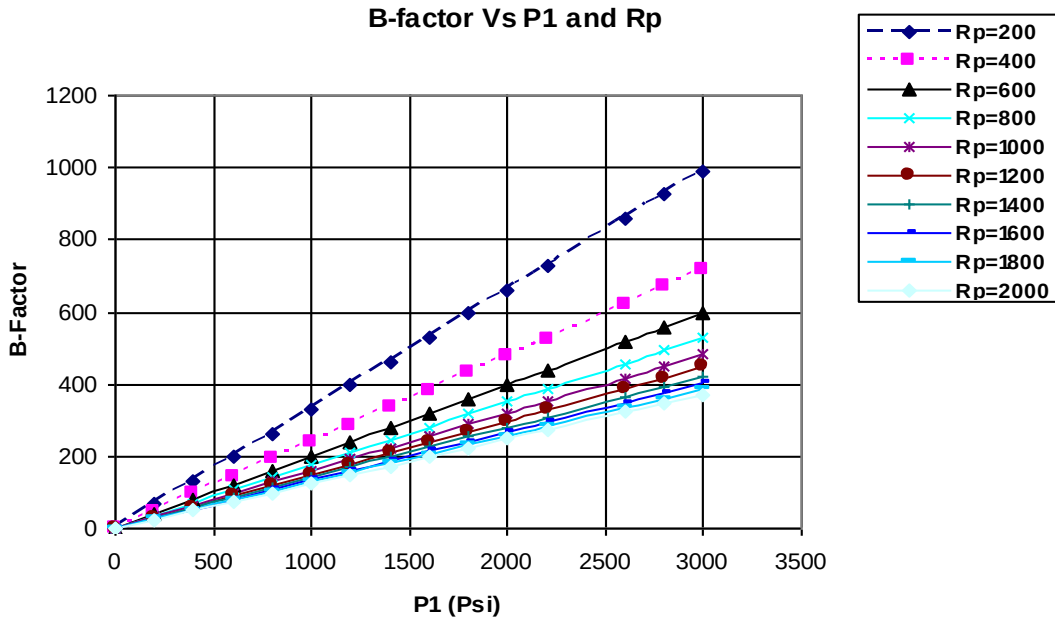

Figure 3. Chart for estimating the beta factor.

X_c, calculate $F(X_{sc})$ from Equation 37 and iterate on X_{sc} until $|F(X_{sc}) - F(X_{sc})_{cal}| < 0.01$.
Iv From (iii) using Equation 36 calculate the desired ΔP.

Example 2

Given the following data, predict the pressure drop across the choke.

K	=	1.04	P_1	=	2500 psia
Bo	=	1.01 bbl/STB	T_1	=	560°R - 580°R
r_g	=	0.95	WOR	=	0.0
r_o	=	0.885	Rs	=	0.0 SCF/STB
q_{TP}	=	500 BPD	R	=	500 SCF/STB,
C_D	=	0.95	dc	=	16/64th

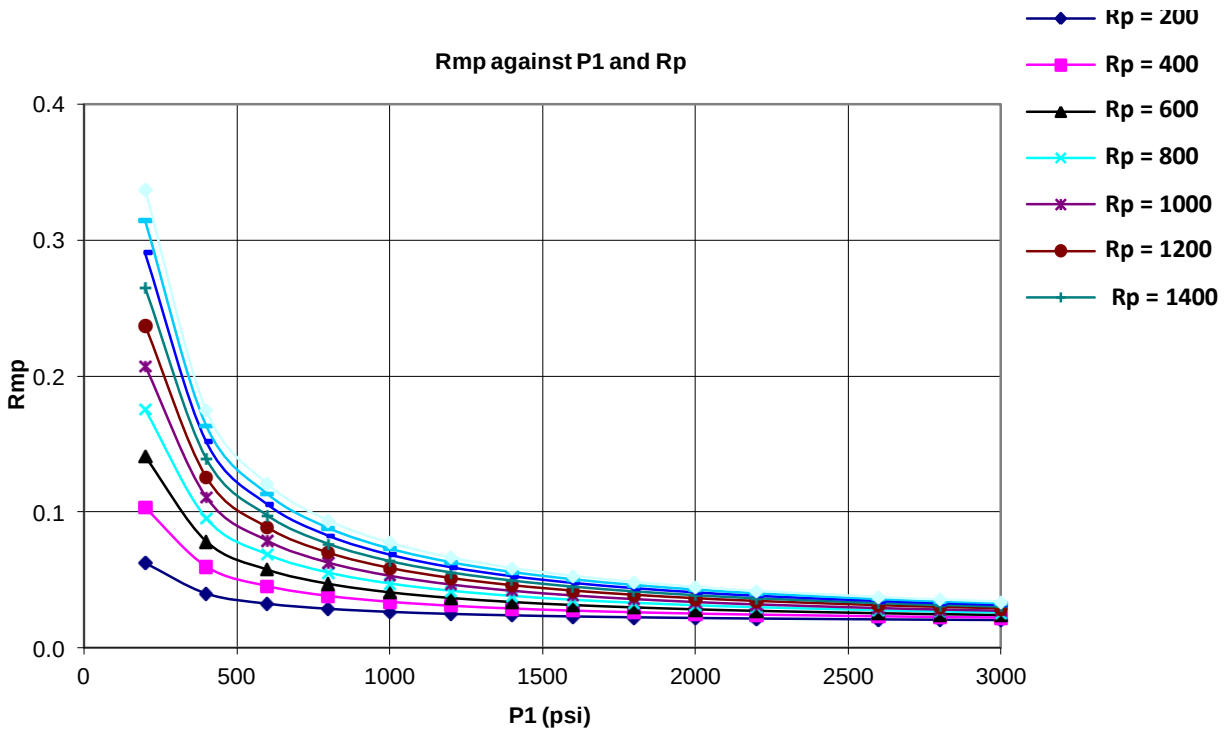

Figure 4. Chart for estimating the specific volume factor.

Solution:

f_b	=	479	(Figure 2)
β	=	680	(Figure 3)
Rmp	=	0.023	(Figure 4)

From Equation 37, $F(X_{sc}) = 0.067$
From Figure 6a, for $F(X_{sc}) = 0.067$, $X_{sc} = 0.95$
From Equation 36, $\Delta P = P_1(1 - X_{sc}) = 125\,psia$

3) Size the valves or chokes

For an expected flow rate q_{TP}, desired pressured drop, fluid characteristics and operating conditions,

i) Obtain $F(X_{sc})$, β, R_{mp}
If you do not know ΔP, then iterate on X_{sc} as in (1) above under calculation of flow capacity
ii) Calculate the base factor, f_b

$$f_b = \frac{q_{TP}}{F(X_{sc})\beta R_{mp}} \qquad (38)$$

(iii) Using Equation 19, calculate the size of the choke or valve

$$d_c = \left(\frac{f_b}{1.97 C_D}\right)^{\frac{1}{2}} \qquad (39)$$

Example 3

Given the following data, size the subsurface choke to be installed in this well.

R	=	1.04	P1	=	2500 psia
B_o	=	1.01 bbl/STB	T1	=	560°R - 580°R
r_g	=	0.95	WOR	=	0.0
ro	=	0.885	Rs	=	0.0 SCF/STB
q_{TP}	=	500 BPD	R	=	500 SCF/STB
C_D	=	0.90			

Solution

β	=	680	(Figure 3)
Rmp	=	0.023	(Figure 4)
F(Xsc)=		0.22	as in Example 1
From Equation 36,	fb	=	145.315
From Equation 37,	dc	=	9/64th inch

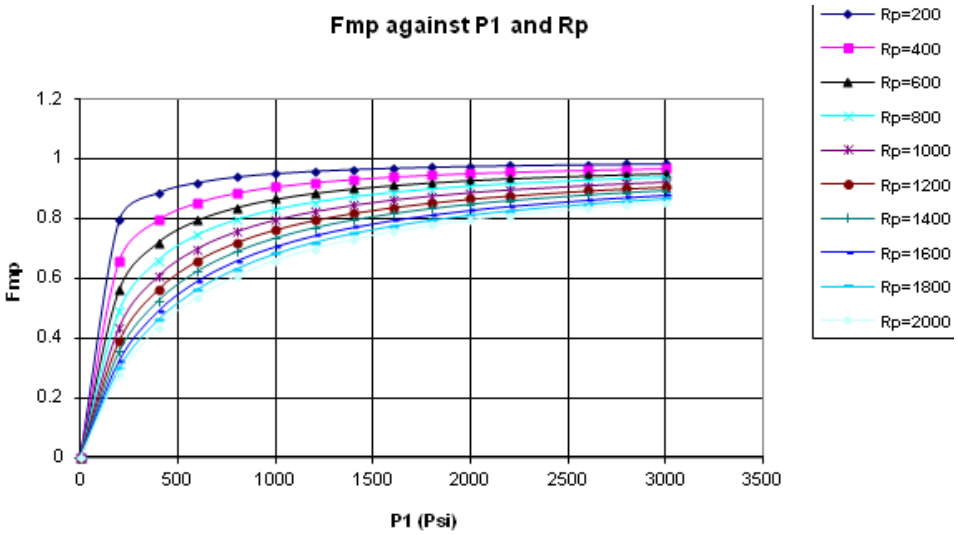

Figure 5. Chart for estimating the multiphase correction factor for oil rate.

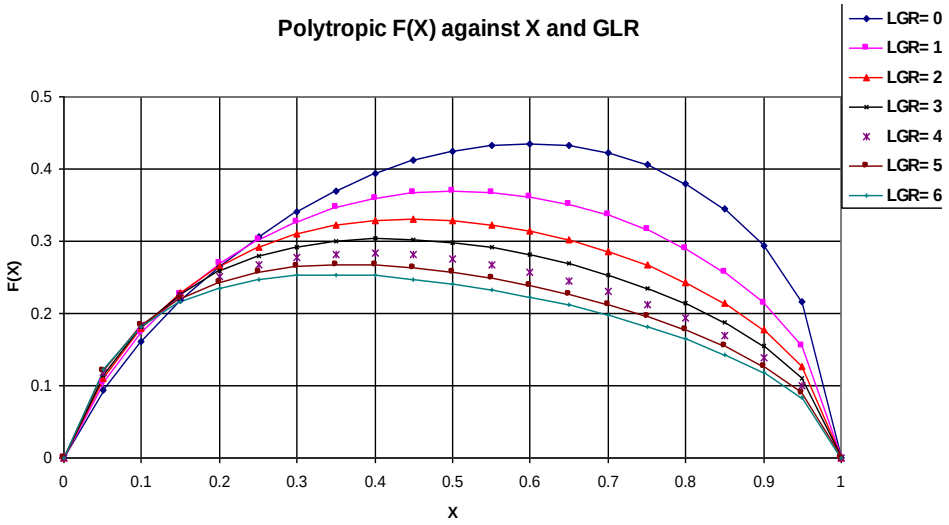

Figure 6a. Prediction of critical multiphase flow for polytropic flow.

Note: After the design calculations, remember to crosscheck with the manufacturing data of valve!

PROBLEMS OF USING SUBSURFACE VALVES AND CHOKES

Sand erosion is a major problem in the design of subsurface valves and chokes because it tends to enlarge the flow opening and make any design calculations valid for short periods of time at best. Thus, it is necessary to monitor the gradual enlargement of choke sizes due to sand erosion. Paraffin deposition is another problem. A qualitative check to know if choke is out of gauge due to sand cutting or paraffin deposition is to use Equation 36 to calculate f_b.

$$f_b = \frac{q_{TP}}{F\left(X_{sc}\right)\beta R_{mp}} \quad \text{(called } f_{bc}\text{)}$$

Compare it with the actual value of f_b (called f_{ba}) calculated using the known choke size in the hole. This can be done as frequently as possible particularly with problematic wells. A wide departure means the valve or choke is out of gauge; thus, a change in dc and C_D (which we can assume to be constant).

(i) If $f_{bc} > f_{ba}$ = sand erosion, opening enlarged.
(ii) If $f_{bc} < f_{ba}$ = scale or paraffin blockage of hole.

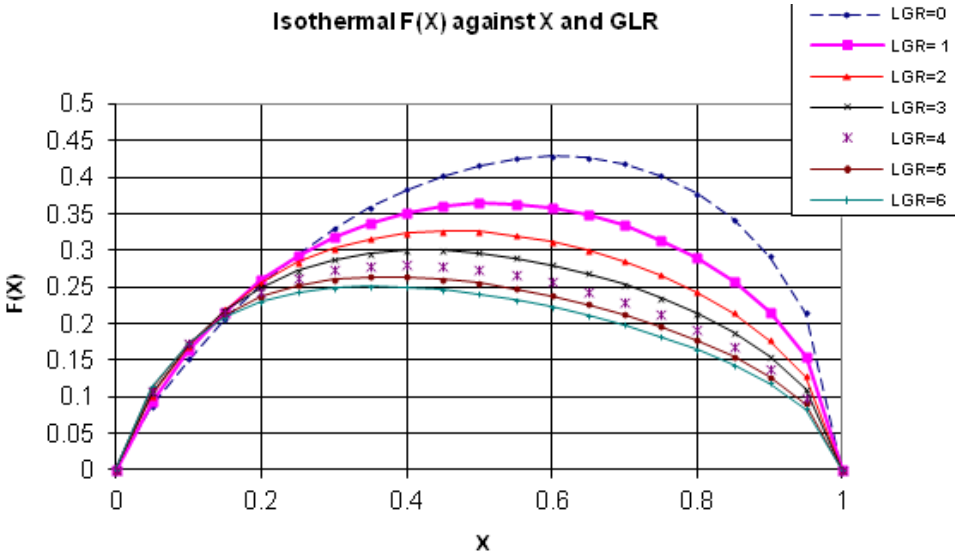

Figure 6b. Prediction of critical multiphase flow for isothermal flow.

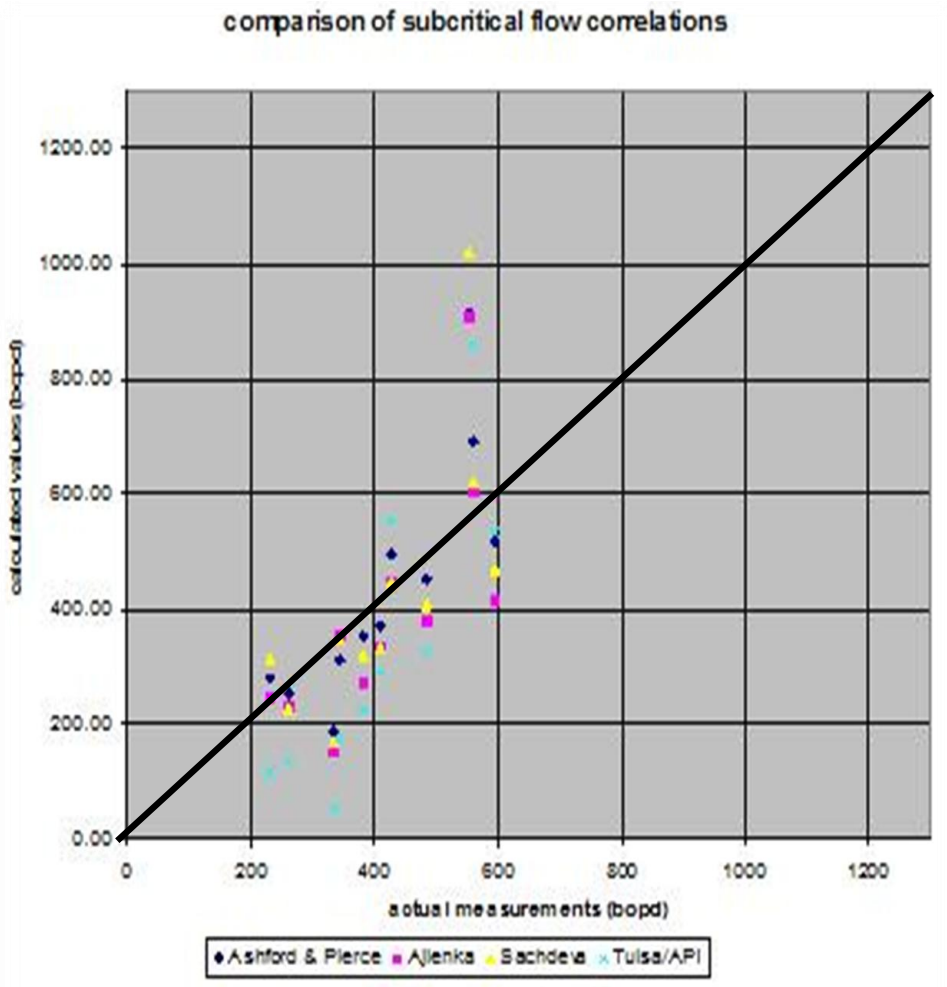

Figure 7. A cross-plot some existing subcritical multiphase flow correlations with this new model. Where AAE is the average absolute error and CD is the discharge coefficient

Another shortcoming of design calculations for long chokes and subsurface valves could result from neglecting effects in the derivation of equations. However, this effect can be incorporated if the effect is significant.

The technology of subsurface valves has progressed from valves run on production string which is impracticable and expensive as each time a valve is to be changed the whole string has to be pulled, to adjustable beans designed to be operated by manipulating rods or tubing from the surface. While possessing certain desirable features, these types of beans have not proved entirely satisfactory because of mechanical difficulties present in any device so extremely sensitive to diameter changes when these changes are attempted from the surface. With improvement in technology, Ros (1960) reported a removable bottom-hole choke which is run and pulled under pressure on wireline and may be set at any desired level in a string of tubing. It has a slip-packer arrangement containing a replaceable position bean. However, it takes more time to prepare and anchor in high pressure wells. With recent technological advances, chokes can be controlled and retrieved using wireline at the surface.

Conclusions

1) A simple dynamic method of evaluating subcritical multiphase flow through down-hole safety valves (storm chokes) is presented.
2) The method is flexible and can be used for both continuous gas phase flow and continuous liquid phase flow
3) Both isothermal and polytropic expansion of the gaseous phase are considered.
4) Method is practical and can be used in the field. It can also be automated.

Conflict of Interest

The author(s) have not declared any conflict of interest.

REFERENCES

Ajienka JA (1984). The Generation and Application of Phase Correlation Factors in Multiphase Flow Metering. Graduate Seminar, Department of Petroleum Engineering University of Port Harcourt, Port Harcourt, Nigeria.

Ajienka JA (1985). An evaluation of multiphase flow through restrictions, M. Eng. Thesis, University of Port Harcourt, Port Harcourt Nigeria.

Ajienka, JA, Ikoku CU (1987). A generalized model for multiphase flow metering, SPE-17174-MS, presented at the Tenth Annual International Conference of Society of Petroleum Engineers (SPE), Lagos, Nigeria.

Al-Attar HH (2009). New correlations for critical and subcritical two-phase flow through surface chokes in high-rate oil wells, SPE 120788, presented at SPE Latin American and Caribbean Petroleum Engineering conference, Cartagena, Colombia

Alipchenkov VM, Nigmatulin RI, Soloviev SL, Stonik OG, Zaichik LI, Zaigarnik YA (2004). A three-fluid model of two-phase dispersed-annular flow. Int. J. Heat Mass Transf. 47:5323-5338.

Ashford FE (1974). An evaluation of critical multiphase flow performance through wellhead chokes. J. Petr. Technol. 26(08):843-850.

Ashford FE, Pierce PE (1975). The determination of pressure drops and flow capacities in downhole safety valves (Storm Chokes). J. Petr. Tech. 27(09):1145-1152.

Beggs HD, Brill JP (1984). Two-phase flow in pipes. http://books.google.co.uk.

Binder RC (1955). Fluid mechanics. Prentice-Hall, N. Y. 3rd Edition

Brown KE (1984). The Technology of Artificial Lift Methods. PPC Books, 3:253-260

De Rosis A (2014). A lattice Boltzmann model for multiphase flows interacting with deformable bodies. Adv. Water Res. 73:55-64.

De Rosis A (2014). Harmonic oscillations of laminae in non-Newtonian fluids: A lattice Boltzmann-immersed Boundary approach. Adv. Water Res. 73:97-107.

Elgibaly AAM, Nashawi IS (1998). New correlations for critical and subcritical two-phase flow through wellhead chokes. J. Can. Pet. Technol. 37(6):36-43.

Falcucci G, Ubertini S, Succi S (2010). Lattice Boltzmann simulations of phase-separating flows at large density ratios: The case of doubly-attractive pseudo-potentials. Soft Matter 6(18):4357-4365.

Fortunati F (1972). Two-phase flow through wellhead chokes. SPE-3742-MS presented at the SPE European Spring Meeting Amsterdam, Netherlands.

Gilbert WE (1954). Flowing and gas-lift well performance. API 801-30H presented at the spring meeting of the Pacific Coast District, Division of Production, American Petroleum Institute Los Angeles, California USA.

Guo B, Al-Bemani AS, Ghalambor A (2007). Improvement in Sachdeva's multiphase choke flow model using field data. J. Can. Petr. Technol. 46(05):22-26.

Kataoka I, Ishii M, Nakayama A (2000). Entrainment and deposition of droplets in annular two-phase flow. Int. J. Heat Mass Transf. 32(9):1573-1589.

Nind TEW (1981). Principles of oil well production. McGraw-Hill, N.Y. 2nd Edition.

Olson RM (1980). Essentials of engineering fluid mechanics. Harper & Row, University of Michigan. 4th Edition.

Poetmann EH, Beck RL (1963). New charts developed to predict gas-liquid flow through chokes. World Oil, 51-95.

Quin Z, Batra R (2009). Local slamming impact of sandwich composite hulls. Int. J. Solids Struct. 46:2011-2035.

Ros NCJ (1960). An analysis of critical simultaneous gas/liquid flow through a restriction and its application to flow metering. Appl. Sci. Res. A. 9(5):374-388.

Ros, NCJ (1961). Simultaneous flow of gas and liquid as encountered in well tubing. J. Petrol. Technol. 13.10 (1961): 1-037.

Ross JS (1932). Recent development and use of bottomhole choking. Trans. AIME 98(01):332-341.

Sachdeva R, Schmidt Z, Brill JP, Blais RM (1986). Two-phase flow through chokes. SPE-15657-MS, presented at the SPE 61st Annual Technical Conference and Exhibition, New Orleans, Louisiana.

Stevanovic V, Studovic M (1995). A simple model for vertical annular and horizontal stratified two-phase flows with liquid entrainment and phase transitions: One-dimensional steady state conditions. Nucl. Eng. Des. 154(3):357-379.

Takagi K, Dobashi J (2003). Influence of trapped air on the slamming of a ship. J. Ship. Res.47:187-193.

academicJournals

Vol. 5(5), pp. 70-82, November, 2014
DOI: 10.5897/JPGE2014.0194
Article Number: 1DF991748325
ISSN 2141-2677

http://www.academicjournals.org/JPGE

Journal of Petroleum and Gas Engineering

Full Length Research Paper

Transfer matrix technique for determining the resonance conditions in retrieving stuck drill pipes with a top vibratory suspended drive

K. K. Botros*, J. O'Blenes and E. Yajure

NOVA Research and Technology Center, Tesco Corporation, Calgary, Alberta, Canada.

Received 25 April, 2014; Accepted 24 October, 2014

A stuck drill pipe has been recognized as one of the most costly and non-productive challenges in drilling operations. Fishing jars are routinely used to un-lock or loosen the stuck (jammed) pipes which in many cases are expensive and the time taken to complete the job can reach several days of continuous jarring. The use of surface mounted vibratory systems has offered an alternative cost effective means to free the stuck pipes. Almost all of these systems are based on eccentric-weight oscillators which impart simple harmonic vertical forces that are transmitted down the pipe via elastic standing waves through the pipe material. A more recent development also uses a suspended oscillator but imparts a sinusoidal oscillatory displacement (rather than force) to the drill pipe at the top surface end, which again is transmitted down the pipe via elastic standing waves. This paper provides a generalized technique for solving the governing equations describing this top oscillatory system and the transmission of the elastic waves along the drill pipe. The transfer matrix technique is used to describe the travelling/standing waves along the pipe, the connecting couplings and the top suspended drive system. Effects of damping are introduced in the complex wave number and at the coupling locations. Examples of drill pipe scenarios are presented to elucidate the usefulness of the technique to determine the resonance condition, that is, the excitation frequencies for maximum retrieving forces at the stuck end, for any given drill pipe geometry. The resulting force amplitudes at the top driver end and the resulting retrieving forces imparted at the stuck end are quantified for any given imposed displacement amplitude at the drive end. A more complex system involving a drill pipe, spear and an elastic liner is also described where the transfer matrix technique is demonstrated to be an effective means to determine the overall system dynamics and resonance conditions.

Key words: Drilling, drill pipe, spear, liners, solid elastic dynamic, elastic waves.

INTRODUCTION

Drilling or fishing jars have been known and used almost since the start of the drilling industry (Gonzalez, 1987). They are classified as mechanical or hydraulic jars, the operations of which are similar in that they both deliver

*Corresponding author. E-mail: Kamal.Botros@novachem.com.

approximately the same impact blow. Jars are designed to be reset by simple string manipulation and are capable of repeated operation or firing before being recovered from the well. As such, they require downhole tool intervention such as spears, over-shots, taper taps, wash-over pipes, etc. Jarring operations may require anywhere from a few to sometimes thousands of impacts to release a fish, and the total time involved for a successful jarring operation can reach over 50 h of continuous impacts (Gonzalez et al., 2007, 2009). Therefore, operations involving jarring usually last days, sometimes weeks, resulting in a considerable loss of productive rig time (Scolfield et al., 1992).

An alternative method of freeing a stuck drill pipe is by means of surface mounted vibratory systems, which perhaps originated in the 1940s, and probably stemmed from the use of vibration to drive pilings. The early use of vibration for driving and extracting piles was confined to low frequency operation; that is, frequencies less than the fundamental resonant frequency of the system and consequently, although effective, the process was only an improvement on conventional hammer equipment. Early patents of this concept are by Bodine (1961, 1987, 1993) which introduced the concept of resonant vibration that effectively eliminated the reactance portion of mechanical impedance, thus leading to the means of efficient sonic power transmission. Another patent along the same concept is by Vogen (1986). The first published work on this technique was outlined by Gonzalez (1987) and was demonstrated by Baker Oil Tools (1994). It is based on surface mounted vibratory systems, whereby eccentric-weight oscillators impart simple harmonic vertical forces that are transmitted down the pipe via elastic standing waves through the pipe material. A derivative of this concept is a suspended oscillator but imparts a sinusoidal oscillatory displacement (rather than force) to the drill pipe at the top surface end, which again is transmitted down the pipe via elastic standing waves.

The present paper provides a generalized technique in solving the governing equations describing these top oscillatory systems and the transmission of the elastic waves down the drill pipe. The transfer matrix technique is used to describe the travelling/standing waves along the pipe, the connecting couplings and the top suspended drive system. Effects of damping are introduced in the complex wave number and at the coupling locations. Examples of drill pipe scenarios are presented to demonstrate the usefulness of the technique to determine the resonance condition, that is, the excitation frequencies for any given drill pipe geometry.

DESCRIPTION OF ELASTIC WAVE MOTION IN LONG RODS

The governing equation for the elastic wave motion in a long, thin rod and the basic propagation characteristics will be described. Consider a straight, prismatic rod of a cross–sectional areas *S* as shown in Figure 1. The coordinate *x* refers to an axial distance along the rod, while *u*(*x,t*) represents the longitudinal displacement at location *x* and time *t*.

The equation of motion applied to the differential element (*dx*) can be written as (Graff, 1975):

$$\rho \frac{\partial^2 u}{\partial t^2} = -\frac{\partial \sigma}{\partial x} + q - \tau D \quad (1)$$

where: *D* = pipe (or rod) outside diameter; *q* = body force per unit volume of the pipe material; *t* = time; *x* = axial distance; *u* = displacement; ρ = density of the rod material; $\sigma =$ stress (positive when compressive); τ = external shear force

Assuming the material behaves elastically and follows a simple linear Hooke's law (Mead, 1975 and Gei, 2010):

$$\sigma = -E\,\varepsilon = -E\frac{\partial u}{\partial x} \quad (2)$$

Where: ε = strain (positive in the x-direction); σ = stress (positive when compressive); *E* = elastic modulus of the rod material.

The negative sign in Equation (2) is imposed because the stress (σ) is defined as positive when compressive. Substituting Equation (2) in Equation (1), we get:

$$\frac{\partial^2 u}{\partial t^2} = c_o^2 \frac{\partial^2 u}{\partial x^2} + q - \tau D \quad (3)$$

Where, c_o is the speed of elastic wave in the rod material defined as:

$$c_o = \sqrt{\frac{E}{\rho}} \quad (4)$$

TRANSFER MATRIX TECHNIQUE

Now, we will introduce the concept of the transfer matrix [T.M.] technique to facilitate the solution of the above wave equation for elastic rods, and extend it to mechanical systems involving mass-spring-damping.

Transfer matrix for a uniform section of elastic rod

If we neglect for a moment the body force (*q*) and the external damping force (τ) in Equation (3), it reduces to the fundamental wave equation, namely:

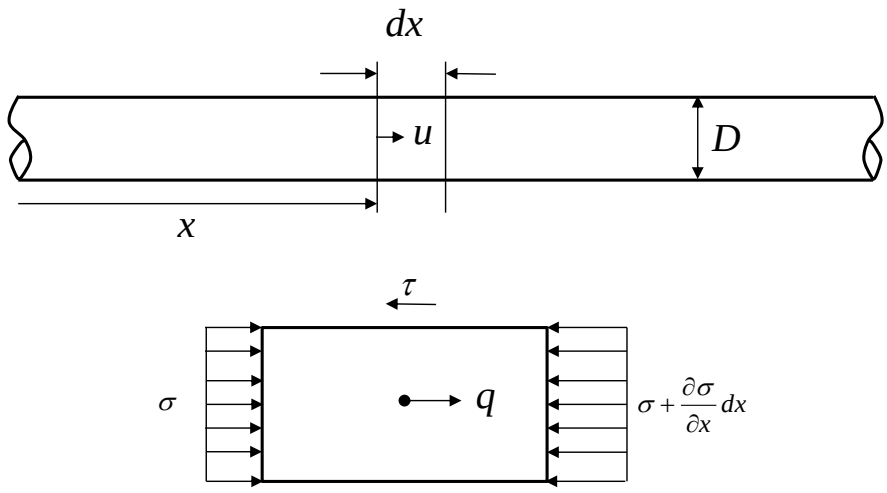

Figure 1. Definition of parameters along an elastic thin rod, and compressive stresses acting on a differential element (*dx*).

$$\frac{\partial^2 u}{\partial t^2} = c_o^2 \frac{\partial^2 u}{\partial x^2} \quad (5)$$

or

$$\frac{\partial^2 \sigma}{\partial t^2} = c_o^2 \frac{\partial^2 \sigma}{\partial x^2} \quad (6)$$

The form of solution of Equation 5 for the displacement *u*can be obtained by the method of separation of variables (Arfken, 2005) in that it can described as a product of a function *X(x)* which depends only on the distance (*x*) and a harmonic function $e^{i\omega t}$ which depends on time and frequency ω (where ω = *2πf*; *f* is the frequency in Hz), that is,

$$u(x,t) = [a\, e^{-ik_o x} + b\, e^{+ik_o x}]e^{iwt} \quad (7)$$

Likewise, the stress (*s*) and the velocity $v(x,t) = \frac{\partial u}{\partial t}$ can also be expressed by similar functions in the form:

$$\sigma(x,t) = [a\, e^{-ik_o x} + b\, e^{+ik_o x}]e^{iwt} \quad (8)$$

and

$$v(x,t) = \frac{1}{\rho_o c_o}[a\, e^{-ik_o x} - b\, e^{+ik_o x}]e^{iwt} \quad (9)$$

Where: $k_o = \omega / c_o$ is the wave number.

Introducing the compressive force (f = σ*S*), where *S* is the cross-sectional area of the rod, Equations (8) and (9) can be written as:

$$\mathrm{f}(x,t) = [a\, e^{-ik_o x} + b\, e^{+ik_o x}]e^{iwt} \quad (10)$$

And

$$v(x,t) = \frac{1}{\rho_o c_o S}[a\, e^{-ik_o x} - b\, e^{+ik_o x}]e^{iwt} \quad (11)$$

The term $\rho_o c_o S = Z_o$ is known as the mechanical characteristic impedance of the elastic rod.

Now, we shall introduce the concept of the transfer matrix [T.M.]. The transfer matrix relates the force and velocity amplitudes at two stations (1) and (2) along a straight rod as shown in Figure 2, in the form of a 2x2 matrix:

$$\begin{bmatrix} F_1 \\ V_1 \end{bmatrix} = \begin{bmatrix} A & B \\ C & D \end{bmatrix} \begin{bmatrix} F_2 \\ V_2 \end{bmatrix} \quad (12)$$

Where the 2x2 matric on the R.H.S. of the above equation is called the transfer matrix whose elements (*A, B, C* and *D*) are all complex numbers. They can be obtained by writing Equations (10) and 11 at the two stations (1) and (2), and substituting *x=0* at station (1) and *x=L* at station (2), and solving for the constants a and b in terms of (F_1, V_1), and (F_2, V_2). Here (F_1, V_1), and (F_2, V_2) are the amplitude of compressive force and velocity oscillations at stations (1) and (2), respectively, which are also complex numbers, that is,

Figure 2. Relationship between amplitudes of force and velocity at different stations along elastic rod.

$$F_1(x=0,t)=F_1 e^{iwt};\ F_2(x=L,t)=F_2 e^{iwt} \tag{13}$$

and

$$v_1(x=0,t)=V_1 e^{iwt};\ v_2(x=L,t)=V_2 e^{iwt} \tag{14}$$

After some arithmetic manipulation, and replacing the exponential terms by trigonometric functions, we obtain:

$$\begin{bmatrix} F_1 \\ V_1 \end{bmatrix} = \begin{bmatrix} \cosh(kL) & Z_o \sinh(kL) \\ \frac{1}{Z_o}\sinh(kL) & \cosh(kL) \end{bmatrix} \begin{bmatrix} F_2 \\ V_2 \end{bmatrix} \tag{15}$$

Where: $k = ik_\circ = i\frac{\omega}{c_o}$

The 2x2 matrix on the RHS of Equation (15) is the [T.M.] of a straight section of elastic rod (drill pipe), which is expressed as:

$$[T.M.]_{rod} = \begin{bmatrix} \cosh(kL) & Z_o \sinh(kL) \\ \frac{1}{Z_o}\sinh(kL) & \cosh(kL) \end{bmatrix} \tag{16}$$

The above $[T.M.]_{rod}$is very useful in facilitating analysis of the dynamic response of a drill pipe subjected to oscillatory force or displacement at the top end, while the bottom end is stuck as depicted in the simple drill pipe schematic shown in Figure 3. Here, station (1) is the top end of the drill pipe while station 2 is the bottom (stuck) end. In this case, the boundary condition at station (2) is V_2=0. Hence, from Equations (12) and (15), the mechanical impedance at station (1) is:

$$Z_1 = \frac{F_1}{V_1} = (\frac{A}{C})_{fromEq.11} = [Z_o \coth(kL)]_{fromEq.14} \tag{17}$$

Equation (17) is plotted as function of frequency of the driving oscillatory system on top for drill pipe parameters shown in the Figure. With the aid of the [T.M.] expression of Equation (15), it can be shown that when the top end of the drill pipe is excited by an oscillatory force of amplitude F_1, the force amplitude exerted at the bottom (stuck) end, F_2, is maximum when impedance Z_1 is at minima, e.g. at frequencies = 0.41, 1.23 Hz, etc. in the example of Figure 4. That is when the length of the drill pipe (L) is equal to odd multiples of $\lambda/4$ (where λ is the wave length = c_o/f). Conversely, when the top is excited by an oscillatory displacement (or velocity of amplitude V_1, the force amplitude exerted at the bottom (stuck) end, F_2, is maximum when impedance Z_1 is at maxima, e.g. at frequencies = 0.82, 1.64 Hz, etc. also in the example of Figure 4. That is when the length of the drill pipe (L) is equal to even multiples of $\lambda/2$.

Figure 5 shows the force amplitudes (F_1 and F_2) resulting from exciting the top end of a drill pipe with an oscillatory displacement of amplitude X_1 = 0.0254 m (1 in), that is, $V_1 = i\omega X_1$. Since the bottom end is assumed stuck, V_2 = 0, and hence Equation (15) can be solved for the amplitudes of forces (F_1 and F_2) shown in Figure 5. The maximum force amplitude at the stuck end of the drill pipe is realized when the displacement excitation frequency at the drive end is 0.81 Hz, that is, when Z_1 is at maximum. Conversely, if the top end is excited with an oscillatory force (as in the case of an eccentric rotating weight), the maximum ratio of force amplitudes (F_2/F_1) is realized at f = 0.41 Hz, that is, when Z_1 is at minimum. Note that the magnitude of F_2at this frequency is simply equal to $i\omega X_1 Z_0$, according to Equation (15) since $\sinh(kL)$ = 1. Note also the overall trend of increasing the amplitude of the force F_2 with frequency which is due to the fact that V_1 is linearly increasing with frequency for the same amplitude of displacement X_1.

Finally, the effect of damping due the shear force (τ) in Equation (1) can be accounted for in the transfer matrix solution of the wave equation via introducing a real parameter (α) in the complex wave number as a damping parameter, or a damping coefficient (ξ) in the form:

$$k = (\alpha + ik_\circ) = \frac{\omega}{c_o}(\xi + i) \tag{18}$$

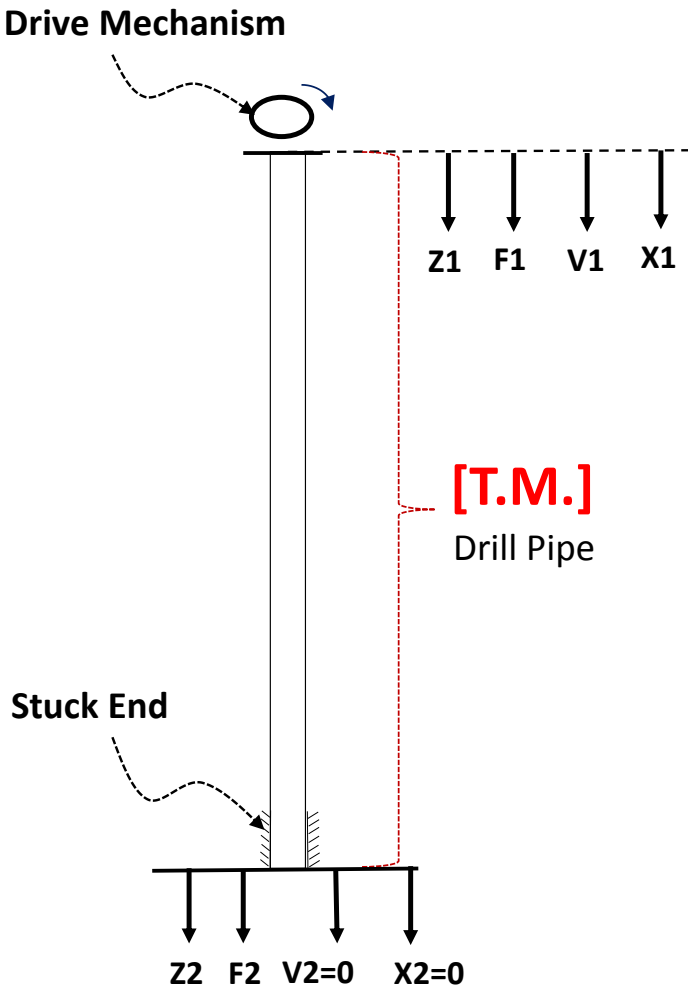

Figure 3. Simple drill pipe stuck at the bottom end and a vibrator at the top end.

Drill Pipe Parameters:		
Drill Pipe O.D.	5.5 in	0.1397 m
Drill Pipe W.T.	0.415 in	0.010541 m
Drill Pipe I.D.	4.67 in	0.118618 m
Cross-Sectional Area	6.62962 in^2	0.004277 m^2
Length of Drill Pipe	10000 ft	3048 m
Elastic Modulus	28275 kpsi	195 GPa
Density	485.917 lb/ft^3	7800 kg/m^3
Speed of Elastic Wave	16374.8 ft/s	5000 m/s

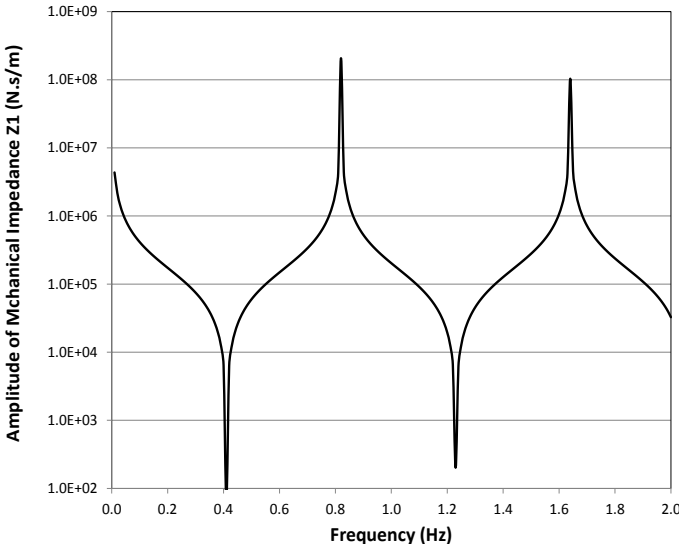

Figure 4. Example of amplitudes of mechanical impedance at the top end of a stuck drill pipe (Ideal System, that is, no damping, no coupling).

Transfer matrix for a coupling with inherent stiffness and damping

Typically, drill pipe segments are connected via couplings which affect the transmission and reflection characteristics of the elastic wave motion in the connected segments. Therefore it is necessary to derive a [T.M.] for these couplings to be combined with the [T.M.] of the respective connecting drill pipe segments (Lin, 1962). Figure 6 shows one type of these coupling where it can generally be represented by a mass-spring-damping system. The quest here is to develop a [T.M.] relating the forces and velocities at stations (2) and (3) in the form:

$$\begin{bmatrix} F_2 \\ V_2 \end{bmatrix} = \begin{bmatrix} A_2 & B_2 \\ C_2 & D_2 \end{bmatrix} \begin{bmatrix} F_3 \\ V_3 \end{bmatrix} \tag{19}$$

The equation of motion for the system depicted in Figure 6 can be written as (Harris and Crede, 1976):

$$F_2 - F_3 = (i\omega m)\, V_1 \tag{20}$$

Where;

$$F_3 = -i\frac{k}{\omega}(V_2 - V_3) + c(V_2 - V_3) \tag{21}$$

And with some mathematical manipulation we get:

$$\begin{bmatrix} F_2 \\ V_2 \end{bmatrix} = \begin{bmatrix} 1 + \dfrac{i\omega m}{(c - \dfrac{ik}{\omega})} & (i\omega m) \\ \dfrac{1}{(c - \dfrac{ik}{\omega})} & 1 \end{bmatrix} \begin{bmatrix} F_3 \\ V_3 \end{bmatrix} \tag{22}$$

Hence the transfer matrix for the coupling element of this type is:

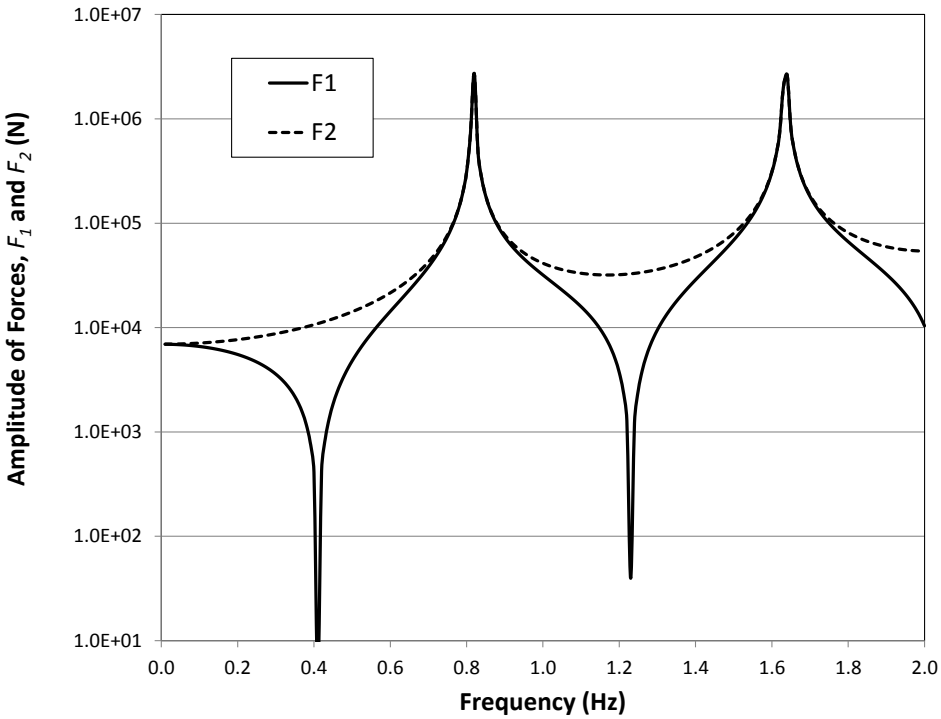

Figure 5. Amplitude of forces at the top and the stuck ends of the ideal drill pipe of Figure 3 (Top end is subjected to oscillatory displacement of amplitude = 0.0254 m).

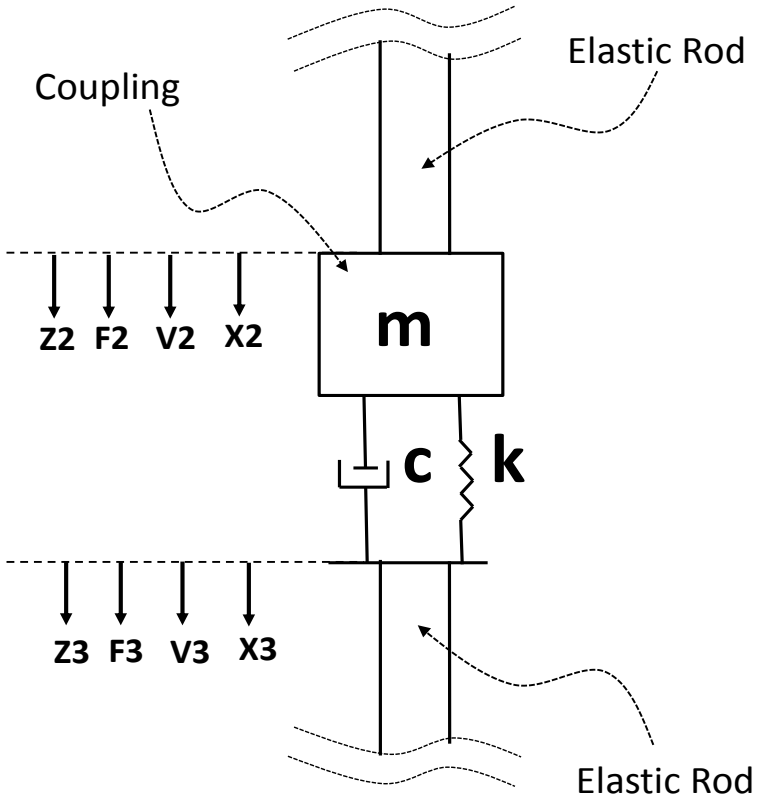

Figure 6. Mass-spring-damping system representing a coupling between two segments of a drill pipe (Type I: Coupling has inherent damping and stiffness).

$$[T.M.]_{coup-1} = \begin{bmatrix} 1+\dfrac{i\omega m}{(c-\dfrac{ik}{\omega})} & (i\omega m) \\ \dfrac{1}{(c-\dfrac{ik}{\omega})} & 1 \end{bmatrix} \quad (23)$$

The above [T.M.] is also applied to elements of the top drive as will be shown later.

It is interesting to note two special cases that can be deduced from the above expression for $[T.M.]_{coup-1}$. The first is the case when station (3) is fixed, that is, $V_3 = 0$. In this case, the impedance Z_2 is reduced to:

$$Z_2 = \frac{A_2}{C_2} = (c + i\omega m - \frac{ik}{\omega}) \quad (24)$$

Which is the well-known expression for the impedance of a mass-spring-damping system mounted on a fixed foundation. The other case is when station (3) is free, that is $F_3 = 0$, hence the impedance Z_2 is reduced to:

$$Z_2 = \frac{B_2}{D_2} = i\omega m \quad (25)$$

Which is the simple equation of motion of the mass element alone.

Transfer matrix for a coupling subjected to external stiffness and damping

Another type of couplings is shown schematically in Figure 7, where the coupling is actually in contact with the borehole which will introduce damping and stiffness between the coupling mass and the surrounding ground. The relating forces and velocities at stations (2) and (3) can be written as follows (Harris and Crede, 1976):

$$F_2 - F_3 = (c + i\omega m - \frac{ik}{\omega})\, V_1 \quad (26)$$

With the condition that:

$$V_2 = V_3 \quad (27)$$

The above two equations can be put in the [T.M.] format as follows:

$$\begin{bmatrix} F_2 \\ V_2 \end{bmatrix} = \begin{bmatrix} 1 & (c + i\omega m - \dfrac{ik}{\omega}) \\ 0 & 1 \end{bmatrix} \begin{bmatrix} F_3 \\ V_3 \end{bmatrix} \quad (28)$$

Hence the transfer matrix for the coupling element of this type is:

$$[T.M.]_{coup-2} = \begin{bmatrix} 1 & (c + i\omega m - \dfrac{ik}{\omega}) \\ 0 & 1 \end{bmatrix} \quad (29)$$

Overall transfer matrix

Having established the transfer matrices for the fundamental elements of a drill pipe, namely: $[T.M.]_{rod}$, $[T.M.]_{coup-1}$ and $[T.M.]_{coup-2}$, it is now possible to determine the overall transfer matrix of a drill pipe system comprising all of these elements. Consider the drill pipe shown in Figure 8 where the drill pipe is composed of three segments connected with couplings of the two types (I and II) as shown.

It can be shown that the relationship between the force and velocity amplitudes at the top end (1) and the bottom end (2) can be expressed via the following overall transfer matrix expression:

$$\begin{bmatrix} F_1 \\ V_1 \end{bmatrix} = \begin{bmatrix} A & B \\ C & D \end{bmatrix}_{overall} \begin{bmatrix} F_2 \\ V_2 \end{bmatrix} = [T.M.]_{overall} \begin{bmatrix} F_2 \\ V_2 \end{bmatrix} \quad (30)$$

Where, the overall transfer matrix, $[T.M.]_{overall}$ is determined from multiplication of the individual transfer matrices corresponding to the elements in the same order, that is:

$$\begin{bmatrix} F_1 \\ V_1 \end{bmatrix} = [T.M.]_{rod1}[T.M.]_{coup1}[T.M.]_{rod2}[T.M.]_{coup2}[T.M.]_{rod3}[T.M.]_{coup3} \begin{bmatrix} F_2 \\ V_2 \end{bmatrix} \quad (31)$$

That is:

$$[T.M.]_{overall} = [T.M.]_{rod1}[T.M.]_{coup1}[T.M.]_{rod2}[T.M.]_{coup2}[T.M.]_{rod3}[T.M.]_{coup3} \quad (32)$$

In the case of a stuck end (that is, at station 2), the impedance at the top end:

$$Z_1 = \frac{A_{overall}}{C_{overall}} \quad (33)$$

The example in the following section will illustrate the application of this overall transfer matrix technique in determining the resonance condition of a stuck drill pipe.

STUCK DRILL PIPE PROBLEM

Now let us consider a stuck drill composed of many

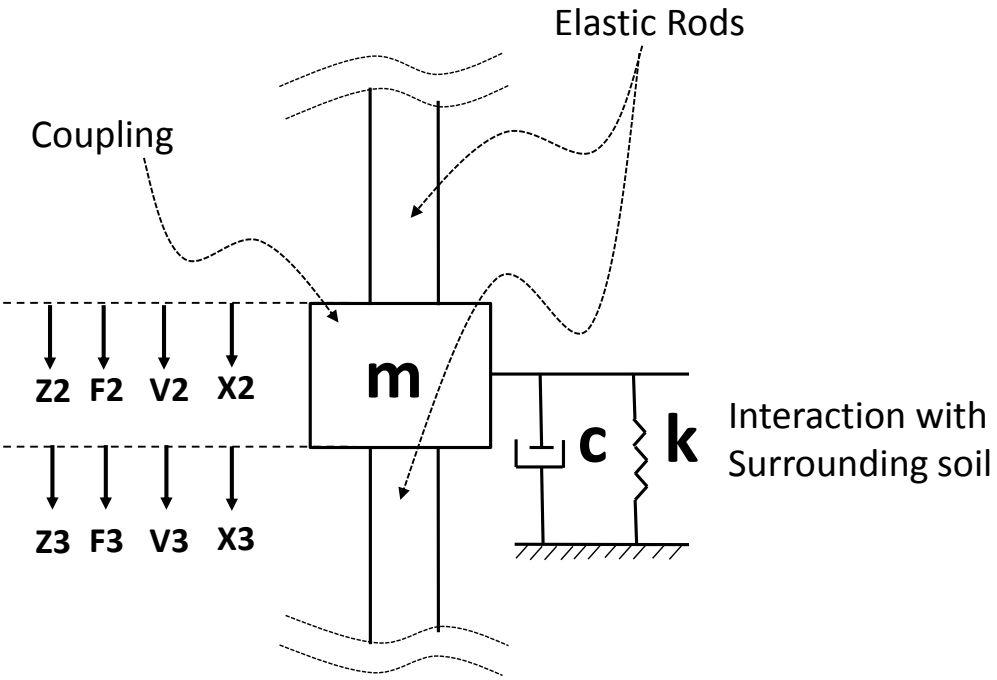

Figure 7. Mass-spring-damping system representing a coupling between two segments of a drill pipe (Type II: Coupling subjected to external damping and compliance.

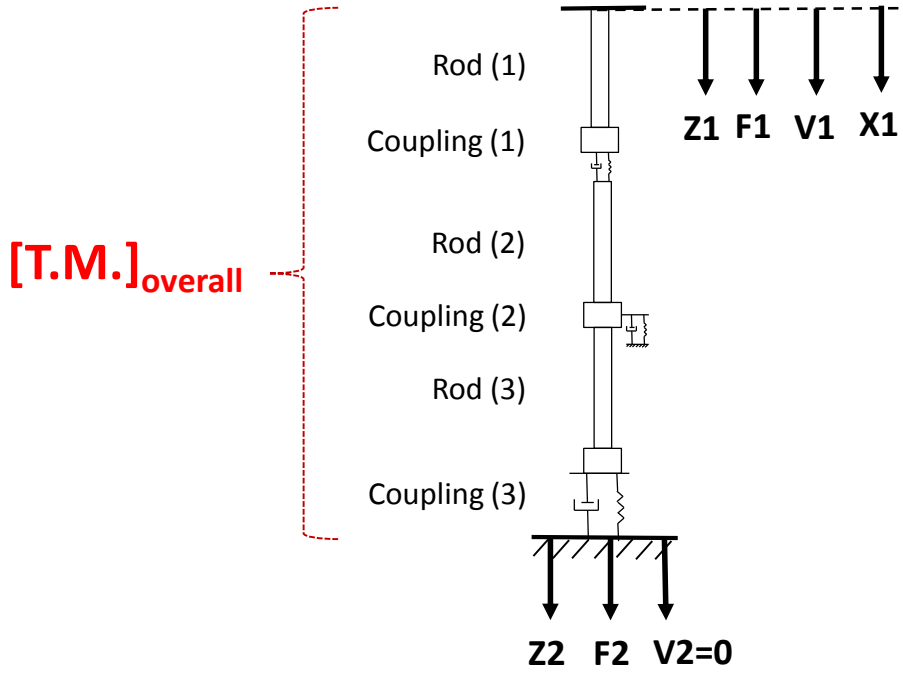

Figure 8. Example of drill pipe segments connected by Type I and Type II couplings.

segments of pipes (could be of different geometries and materials), and couplings of type I or type II connecting these segments as shown on the L.H.S. of Figure 9. Again, the drill pipe is assumed stuck at the bottom end. In order to free this end, a cable-suspended drive is used to generate an oscillatory displacement in a manner such that:

$$X_1 + X_2 = Amp \tag{34}$$

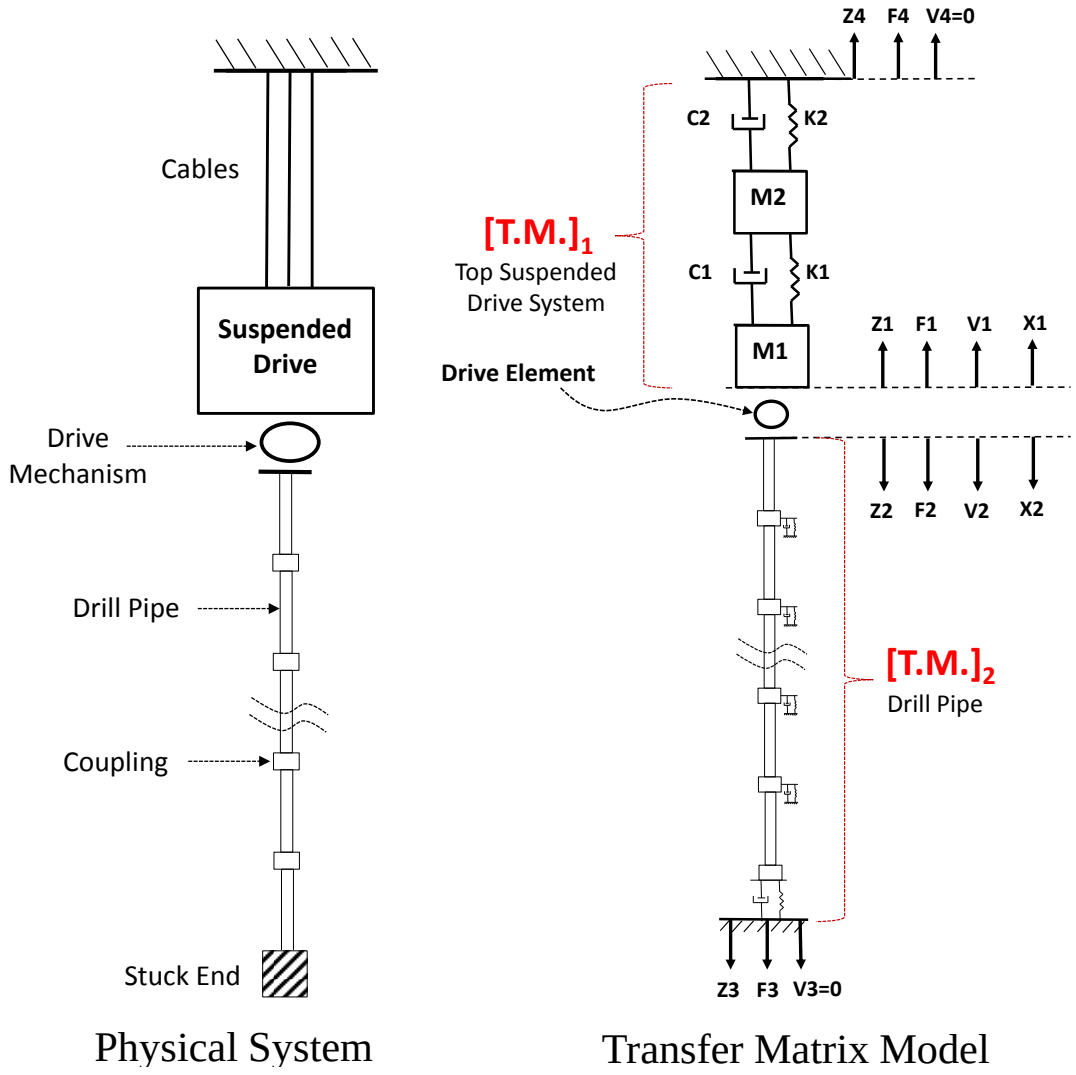

Figure 9. Schematic of the physical system and transfer matrix model depiction of a stuck drill pipe.

Where: *Amp* is a specified amplitude of displacement, X_1 is the amplitude of upward displacement of the suspended drive, while X_2 is the amplitude of displacement of the top end of the drill pipe. The sign convention depicted in Figure 9. The suspended drive can be considered as a two-degree of freedom system as shown on the model schematic on the R.H.S. of Figure 9.

Following the above formulation of the overall transfer matrix, it is possible to obtain both $[T.M.]_1$ and $[T.M.]_2$ by a simple multiplications of the [T.M.]'s corresponding to all of the sub-elements in each, and again, in the correct order, that is,

$$[T.M.]_1 = \begin{bmatrix} A_1 & B_1 \\ C_1 & D_1 \end{bmatrix} \; ; \; [T.M.]_2 = \begin{bmatrix} A_2 & B_2 \\ C_2 & D_2 \end{bmatrix} \tag{35}$$

The corresponding impedances (Z_1 and Z_2) can also be determined since $V_3 = V_4 = 0$. That is:

$$Z_1 = \frac{A_1}{C_1} \; ; \; Z_2 = \frac{A_2}{C_2} \tag{36}$$

Now, substituting $X=V/i\omega$ in Equation (34), we get:

$$\frac{V_1}{i\omega} + \frac{V_2}{i\omega} = \frac{1}{i\omega}\left(\frac{F_1}{Z_1} + \frac{F_2}{Z_2}\right) = Amp \tag{37}$$

And since $F_1=F_2$, Equation (37) becomes:

$$F_1 = F_2 = \frac{i\omega \; Amp}{\left(\frac{1}{Z_1} + \frac{1}{Z_2}\right)} \tag{38}$$

Once F_1 is determined, all other parameters (F_3, V_1, V_2, X_1 and X_2) are determined at any given excitation

Table 1. Parameters of the stuck drill pipe system and suspended drive shown in Figure 9.

System parameters	Values
Suspended mass (M1)	27273 kg
Damping (C1)	160000 N.s/m
Stiffness (K1)	7022190 N/m
Suspended mass (M2)	9091 kg
Damping (C2)	16000 N.s/m
Stiffness (K2)	98310666 N/m
Drill pipe O.D.	0.1397 m
Drill pipe I.D.	0.118618 m
Drill pipe X-Area	0.004277 m^2
Drill pipe overall length	3048 m
Weigh per unit length (including Coulings)	37 kg/m
Drill pipe damping coefficient (ξ)	0.05
Damping at coupling (C)	1600 N.s/m
Stiffness at coupling (K)	0 N/m
Amplitude of *X1 + X2 =Amp*	0.0254 m

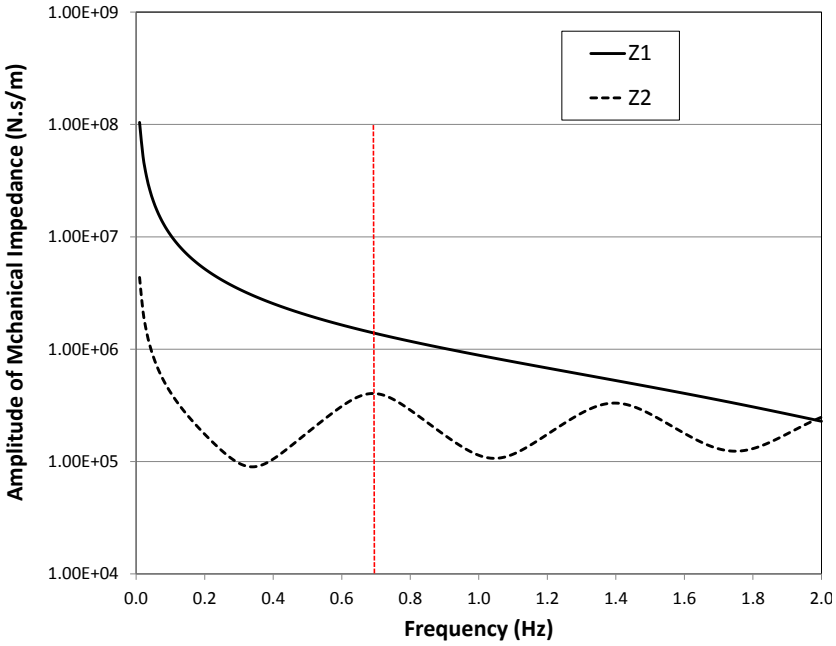

Figure 10. Results of the mechanical Impedances (Z_1 and Z_2) of the drill pipe system shown in Figure 9.

frequency. Table 1 gives values for the relevant parameters for an example drill pipe stuck at a depth of 3048 m (10,000 ft). The drill pipe is divided into 100 segments and a coupling of Type II is placed between each consecutive segments whose mass is combined with 1/3 of the mass of the preceding segment. The resulting impedances Z_1 and Z_2 are shown in Figure 10, the amplitudes of displacements X_1 and X_2 are shown in Figure 11, and the amplitude of the driving force, F_1, and the retrieving force at the stuck end, F_3, in Figure 12.

The magnitude of Z_1 is generally higher than that of Z_2 (Figure 10), which is desirable as it indicates that it is '*easy*' to displace down the top end of the drill pipe than to push up the massive suspended drive. In other words, the mobility (which is the inverse of the impedance) of the drill pipe top end is much greater than the suspended drive. This is manifested in the resulting displacement amplitudes X_1 and X_2 in Figure 11. Note also that at the

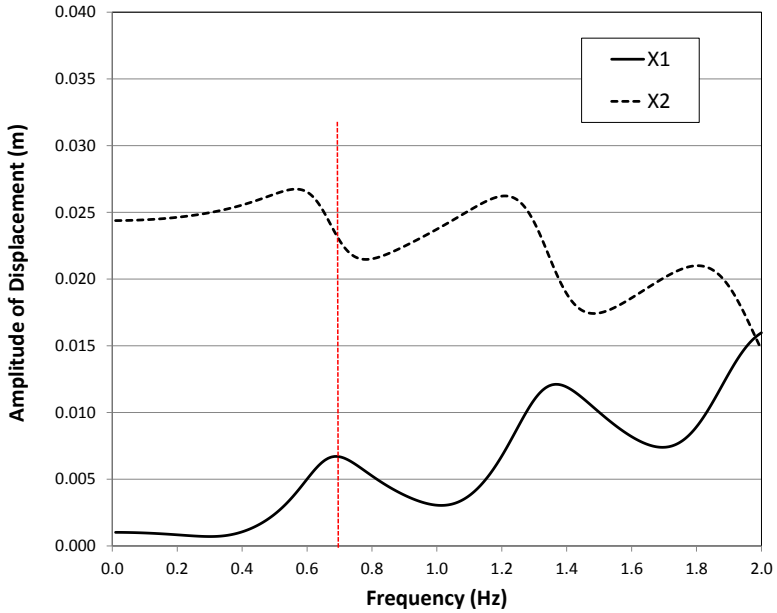

Figure 11. Results of the displacements (X_1 and X_2) of the drill pipe system shown in Figure 9.

desired drive frequency of 0.69 Hz (corresponding to the first maximum impedance in Figure 10), the amplitude of X_1 = 0.0067 m while the amplitude of X_2 = 0.0242 m.

It probably begs the question as to why the frequency at maximum impedance Z_2 is now lower (0.69 Hz) than that in the case of Figure 4 (0.82 Hz) despite the fact that the drill pipe length is the same in both cases (that is, 3048 m). The main reason is that in the present case damping was introduced along the drill pipe (ξ = 0.05) as well as a damping parameter, c, to all of the the couplings. Additionally, the weight of the drill pipe segments and couplings were accounted for in the analysis of this example, while in the example of Figure 4, it was clearly stated that the drill pipe was clear of any damping (that is, ideal). Damping is also manifested in decreasing the force amplitude F_3 than F_2 as shown in Figure 12.

A MORE COMPLEX PROBLEM OF A STUCK LINER

Let us now consider a more complex geometry of a case involving a drill pipe in a liner, where the liner is stuck at the bottom end as depicted in the schematic of Figure 13. The corresponding transfer matrix model system is also shown on the R.H.S of Figure 13. The drill pipe is assumed stuck at the bottom end, while it is rigidly supported at the top surface. To free the liner, the same cable-suspended drive is used to generate an oscillatory displacement at the top end of the drill pipe in a manner similar to the last example, that is, Equation 34. Similarly, it is possible to obtain the overall transfer matrices $[T.M.]_1$, $[T.M.]_2$, $[T.M.]_4$ and $[T.M.]_5$ via simple multiplications of the respective [T.M.]'s corresponding to each of the sub-elements in each sub-system shown in Figure 13, that is,

$$[T.M.]_1 = \begin{bmatrix} A_1 & B_1 \\ C_1 & D_1 \end{bmatrix} \;;\; [T.M.]_2 = \begin{bmatrix} A_2 & B_2 \\ C_2 & D_2 \end{bmatrix}$$
$$[T.M.]_4 = \begin{bmatrix} A_4 & B_4 \\ C_4 & D_4 \end{bmatrix} \;;\; [T.M.]_5 = \begin{bmatrix} A_5 & B_5 \\ C_5 & D_5 \end{bmatrix} \quad (39)$$

The corresponding impedances (Z_1 and Z_4 and Z_5) can also be determined from:

$$Z_1 = \frac{A_1}{C_1} \;;\; Z_4 = \frac{A_4}{C_4} \;;\; Z_5 = \frac{A_5}{C_5} \quad (40)$$

The condition at the spear is such that:

$$F_3 = F_4 - F_5 \;\; and \;\; V_3 = V_4 = -V_5 \quad (41)$$

It follows that:

$$Z_3 = Z_4 + Z_5 \quad (42)$$

Hence:

$$Z_2 = \frac{A_2 Z_3 + B_2}{C_2 Z_3 + D_2} \quad (43)$$

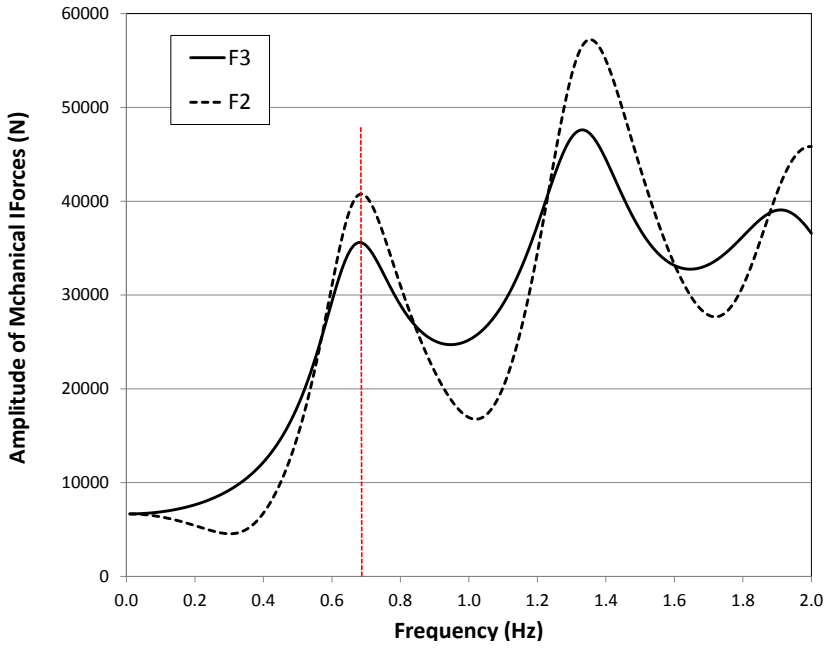

Figure 12. Results of the displacements (F_1 and F_3) of the drill pipe system shown in Figure 9.

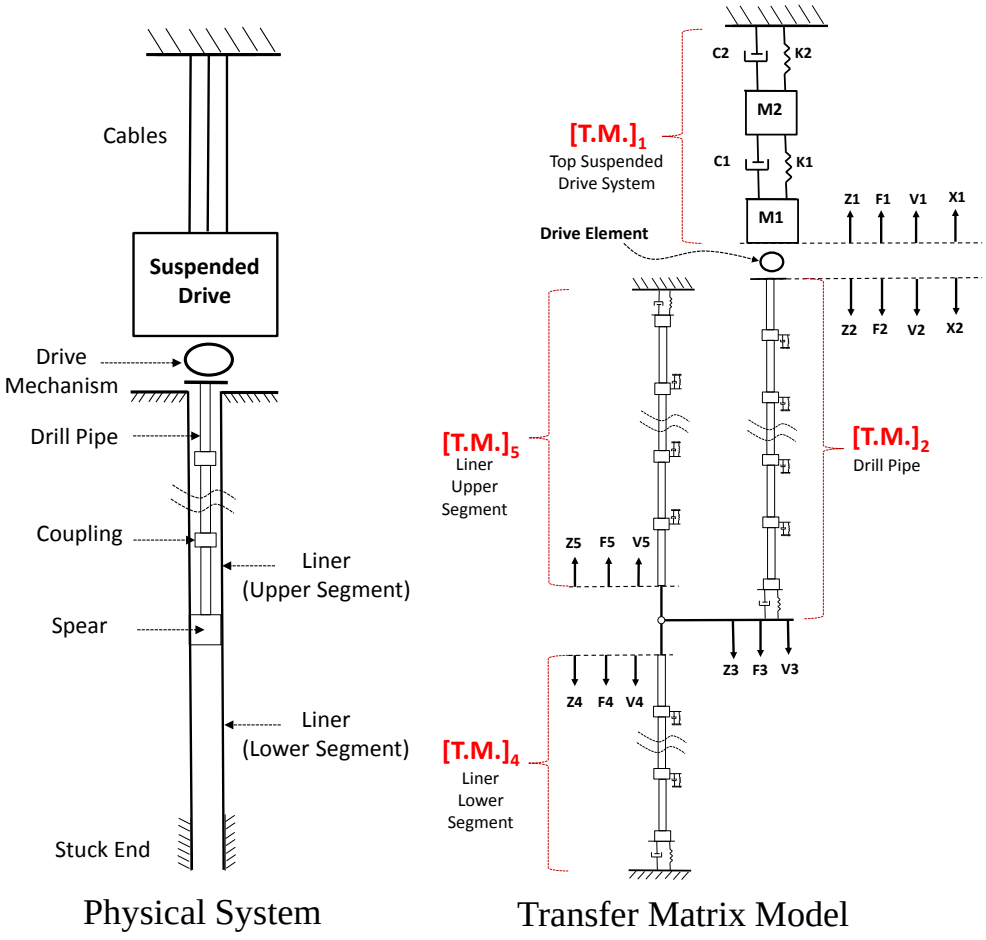

Figure 13. Schematic of the physical system and transfer matrix model depiction of a stuck liner.

Equation 38 is applied to determine the force F_1 and all other amplitudes of impedances, forces, velocity and displacements. It should be remembered that the parameters described in Equations 33 through 43 are all complex numbers.

DISCUSSION

The transfer matrix technique [T.M.] is demonstrated to be a very powerful and useful technique to describe any complex drill pipe/liner dynamic response to a top surface oscillatory drive to retrieve a stuck bottom end of the drilling assembly. The general form of the [T.M.] is a 2×2 matrix whose elements are generally complex numbers. For a drill pipe, the [T.M.] accounts for the length of the drill pipe, its cross sectional area, material properties and effective damping. The [T.M.] for couplings and surface drive elements are derived from the dynamic response of generally mass-spring-damping system. The elements of these 2×2 [T.M.] are also expressed in complex numbers.

Once the [T.M.] corresponding to each element in the system is formulated, the overall system [T.M.] can be obtained. For example elements connected in series (such as drill pipe segments connected via couplings), the overall [T.M.] of the string of drill pipe will be a simple multiplication of the individual [T.M.]'s in the same order as connected. Sign conventions of amplitudes of impedance, force, velocity and displacement, which all are also complex numbers, should be observed in formulating the problem.

It was shown that damping affects the resonance frequency as well as the amplitude of the retrieving forces at the stuck end. Therefore, it is important to accurately quantify all possibilities of damping imposed on the system, whether it is from the ground soil contacting with the mechanical system, or inherent within the actual design of the element.

Finally, it was shown if the vibrator drive at the surface end is imparting an oscillatory force on the drill pipe at the top, the resonance condition for maximum force at the stuck end is corresponding to the minimum impedance at top end. Conversely, if the vibrator is imparting an oscillatory displacement at the top, the resonance condition for maximum force at the stuck end is corresponding to the maximum impedance at top end. Therefore, it is necessary to determine the length of the drill pipe to the stuck end so as to drive the top vibrator close to the resonance frequency for best results.

Nomenclatures: ***A, B, C, D*****,** elements of the 2x2 transfer matrix; ***Amp,*** amplitude of excitation displacement; ***c,*** damping parameter; c_o**,** speed of elastic wave in the drip pipe; ***D,*** pipe (or rod) outside diameter; ***E,*** elastic modulus; ***F,*** force amplitude; ***I,*** $i=\sqrt{-1}$ **,** ***k,*** complex wave number or spring stiffness; k_o**,** wave number; ***L,*** length of drill pipe; ***m,M,*** mass; ***q,*** body force per unit volume of the pipe material; ***S,*** drill pipe cross-sectional area; ***t,*** time; **[T.M.,],** transfer matrix; ***u,*** displacement; ***v,*** velocity; ***V,*** velocity amplitude; ***X,*** axial distance; ***X,*** displacement amplitude; ***Z,*** impedance (=*F/V*); **A,** damping parameter; **ε,** strain (positive in the x-direction); ***F*****,** excitation frequency (Hz); ρ**,** density of the rod material; **σ,** stress (positive when compressive); **τ,** external shear force; ω**,** excitation frequency (rad/s);**ξ,** damping coefficient.

REFERENCES

Arfken GB, Weber HJ (2005). Mathematical Methods for Physicists.6th Edition. Elsevier Academic Press.

Baker Oil Tools (1994). Resonant Systems Product No. 140-52.Product Report number PR/FS/94002/2M/4-94.

Bodine AG (1961). Acoustic Method and Apparatus For Moving Objects Held Tight Within a Surrounding Medium. United States Patent number: 2972380.

Bodine AG (1987). Down hole excitation system for loosening drill pipe stuck in a well. United States Patent 4667742.

Bodine AG (1993). Sonic method and apparatus for freeing a stuck drill string. United States Patent 5234056.

Gei M (2010): Wave propagation in quasiperiodic structures: stop/pass band distribution and pre-stress effects. Int. J. Solids Structures. (47):3067-3075.

Gonzalez O (1987). Retrieving Stuck Liners, Tubing, Casing And Drill Pipe With Vibratory Resonant Techniques. Soc. Petrol. Engrs. Paper # 14759. SPE Drill. Engr. J. 2(3):245-256.

Gonzalez O, Bernat H, Moore P (2007).The Extraction of Mud-Stuck Tubular Using Vibratory Resonant Techniques.SPE Annual Technical Conference and Exhibition. Anaheim, California, U.S.A.

Gonzalez O, Bernat H, Moore P (2009). The Extraction of Stuck Drill Pipe Using Surface Resonant Vibratory Techniques. American Assoc. of Drilling Engineers. National Technical Conference and Exhibition. New Orleans, Louisiana.

Graff KF (1975). Wave Motion in Elastic Solids. Oxford University Press.

Harris CM, Crede E (1976). Shock and Vibration Handbook.2nd Edition. Chapter 10. McGraw Hill.

Lin YK (1962). Free vibrations of a continuous beam on elastic supports. Int. J. Mech. Sci. 4:409-423.

Mead DJ (1975). Wave propagation and natural modes in periodic systems I-mono-coupled systems. J. Sound Vib. (40):19-39.

Scolfield TR, Whelehan OP, Baruya A (1992). A New Fishing Equation. Paper SPE 22380 presented at the SPE International Meeting on Petroleum Engineering held in Beijing, China.

Vogen WV (1986). Method and Apparatus for Removing Stuck Portions of a Drill String. United States Patent 4:574,888.


Journal of
Petroleum and Gas
Engineering
Journal of Mechanical Engineering Research
Journal of Chemical Engineering and Materials Science
Journal of Engineering and Computer Innovations
Journal of Engineering and Technology Research
Journal of Petroleum Technology and Alternative Fuels
academicJournals